

Neutron-induced Fission

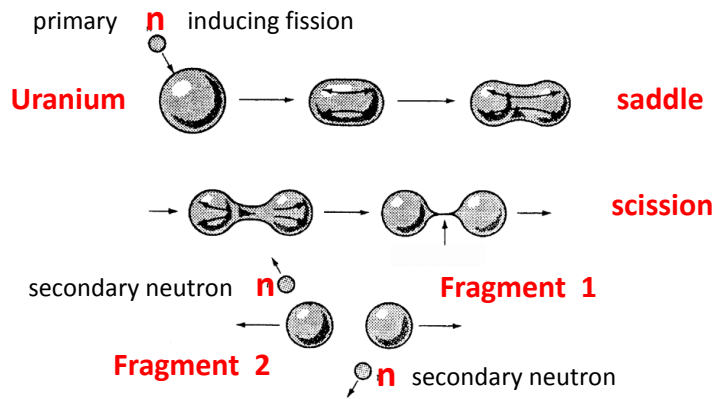
F. Gönnenwein

University of Tübingen / Germany

Neutron-induced Fission I

History:

Neutron-induced fission of Uranium was the reaction leading to the discovery of fission in January of 1939 by O. Hahn and F. Strassmann. In the process a heavy nucleus decays into two fragments of comparable mass. It was discussed by L Meitner in terms of a liquid drop which becomes deformed and which beyond a critical deformation is breaking apart into two pieces, the fission fragments. The figure visualizes the process:



In the multidimensional landscape of deformation the critical deformation of no return to the mono-nucleus shows up as a saddle. With further deformation a situation is reached where the neck joining the two nascent fragments is no longer stable but is breaking apart. The snapping of the neck is called scission. Two fission fragments with similar but in general not equal masses are born. An obvious task in fission physics is hence the measurement of fragment **mass and charge distributions**. The fragments being charged the Coulomb forces will impart them large **kinetic energies**. The study of these energies is a further challenge.

As discovered by the team of F. Joliot and published in March 1939 [von Halban 1939] **secondary neutrons** are created in fission. Finally, in the last stage of fission **gammas** are emitted.

Liquid drop Model:

In September 1939 N. Bohr and J.A. Wheeler published a seminal paper entitled “The Mechanism of Nuclear Fission” [Bohr 1939]. Nuclear fission is interpreted in terms of the Liquid Drop Model. It is up to now the basis for understanding the process.

In the LDM the binding energy B of a nucleus is parameterized as

$$B = a_V A - a_S A^{2/3} - a_C Z^2/A^{1/3} - a_A (N-Z)^2/A \pm \delta/A^{1/2}$$

Volume Surface Coulomb Asymmetry Pairing
 $a_V = 1.56$ $a_S = 17.23$ $a_C = 0.70$ $a_A = 23.29$ $\delta = 12.0$ MeV

When the liquid drop becomes deformed, e.g. from a sphere to a spheroid, only the surface and the Coulomb energy are affected. Small deformations are described by developing the radius vector $R(\theta)$ of the nucleus

$$R(\theta) = R_0[1 + \alpha_2 P_2(\cos\theta)]$$

with P_2 the second Legendre polynomial.

For small deformations α_2 Bohr-Wheeler calculate the surface and Coulomb energies E_S and E_C

$$E_S = E_S^0(1 + \frac{2}{3}\alpha_2^2) \text{ and } E_C = E_C^0(1 - \frac{1}{5}\alpha_2^2)$$

with E_S^0 and E_C^0 the energies for spherical nuclei as given by the LDM. For a spherical nucleus to be stable the

$$\text{decrease in Coulomb energy } \Delta E_C = -\frac{1}{5}\alpha_2^2 E_C^0$$

must be smaller than the

$$\text{increase in surface energy } \Delta E_S = +\frac{2}{3}\alpha_2^2 E_S^0$$

which for the limit of stability yields $|\Delta E_C| = \Delta E_S$ or $E_C^0 = 2E_S^0$.

Bohr-Wheeler therefore introduce the notion of **Fissility x**

$$x = E_C^0 / 2 E_S^0 = \frac{Z^2}{A} / 51.7$$

Only for $x < 1$ nuclei are stable against “immediate “ decay.

Neutron-induced Fission II

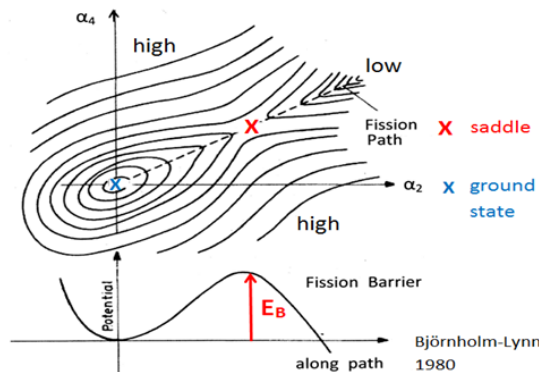
The Fission Barrier:

To calculate for large deformations the deformation energies requires to foresee in the expansion of $R(\theta)$ more Legendre polynomials than just P_2 :

$$R(\theta) = R_0/\lambda [1 + \sum_{n=1} \alpha_n P_n(\cos\theta)]$$

with λ a scale factor ensuring volume conservation.

Bohr-Wheeler succeeded to evaluate the potential energy of deformation as a function of the parameters α_2 and α_4 . At small deformations the energy increases as expected. But the crucial discovery was that in the (α_2, α_4) plane a saddle point is reached at specific α -parameter values. This is illustrated in the figure. Beyond the saddle a path of minimum energy slopes downwards until the nucleus is breaking apart at scission. Fission proceeds along this path marked as a dashed line in the figure. A fissioning nucleus moving along the path has to overcome a potential barrier as shown in the lower part of the figure. The height of this “fission barrier” B_f above the ground state is about 6 MeV in the actinides.

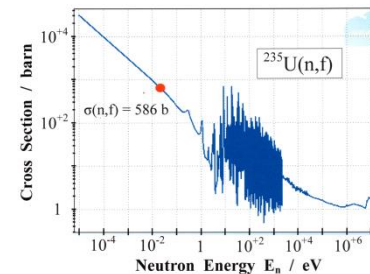


The fission barrier prevents heavy nuclei from immediate decay by fission. However, similar to α -decay, the nucleus has a finite chance to tunnel through the barrier. “Spontaneous fission”, as this process is called, was indeed observed for ^{238}U already in 1940 [Flerov 1940].

Neutron-induced Fission of Fissile Nuclei:

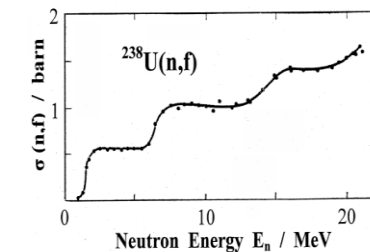
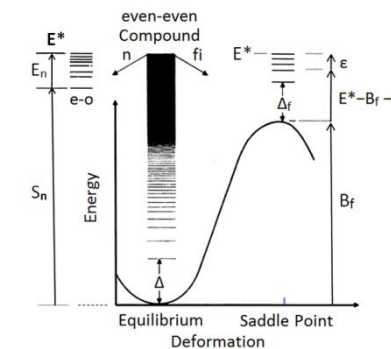
Fission induced by neutrons in actinide nuclei is the best studied fission reaction. Apart from its technological importance this is due to the exceptionally large cross sections for fission of nuclei like ^{235}U by thermal neutrons. The rate dN_f/dt of fission events in a flux of neutrons with density Φ_n is determined by the total number of irradiated target nuclei N_t and the fission cross section σ_f quoted in barns: $1 \text{ b} = 10^{-28} \text{ m}^2$.

$$dN_f/dt = \Phi_n \cdot N_t \cdot \sigma_f$$



In the reaction $^{235}\text{U}(n_{\text{th}},f)$ with thermal neutrons of energy $E_n = 25 \text{ meV}$ the fission cross section $\sigma_f = 586 \text{ b}$ is huge ≈ 340 times the geometrical cross section of ^{236}U .

One of the reasons for the huge σ_f is the large neutron separation energy $S_n = 6.5 \text{ MeV}$ in ^{236}U which exceeds the fission barrier $B_f = 5.6 \text{ MeV}$. For thermal neutrons the excitation energy E^* of the compound is $E^* = S_n > B_f$. The isotope ^{235}U is said to be “fissile”.



In contrast, the most abundant U-isotope ^{238}U has the separation energy $S_n = 4.8 \text{ MeV}$ smaller than the barrier height $B_f = 6.3 \text{ MeV}$. It is non-fissile. To induce fission the incoming neutron energy must be $E_n > 1.5 \text{ MeV}$.

Fragment Mass Distributions

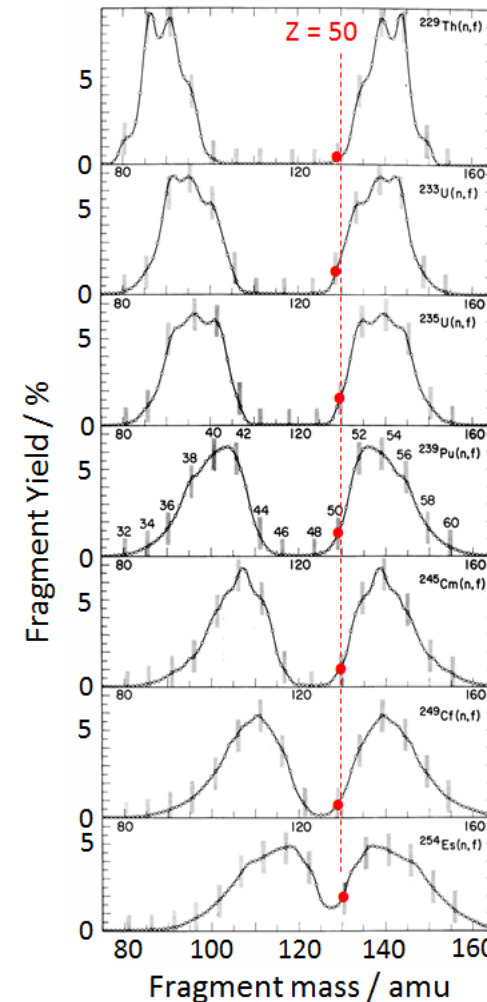
Neutron-induced Fission of Actinides

Neutron-induced fission has almost exclusively been studied with targets in the actinides. The actinides cover the range of elements from Actinium ($Z = 89$) up to Lawrencium ($Z = 103$). In the chart of nuclides they lie in an island of relative stability. There are however only 3 isotopes with lifetimes of $T_{1/2} \approx 10^9$ a or longer. But also these isotopes eventually decay by α -emission or spontaneous fission.

Fission of pre-actinides and post-actinides (superheavy elements) was investigated with light or heavy ions as projectiles or by Coulomb excitation. Valuable information has also come from photofission with photons produced by bremsstrahlung.

In each of the above mass regions of the chart of nuclides the fragments have characteristic properties. Notably their mass distributions are specific and therefore of prime interest.

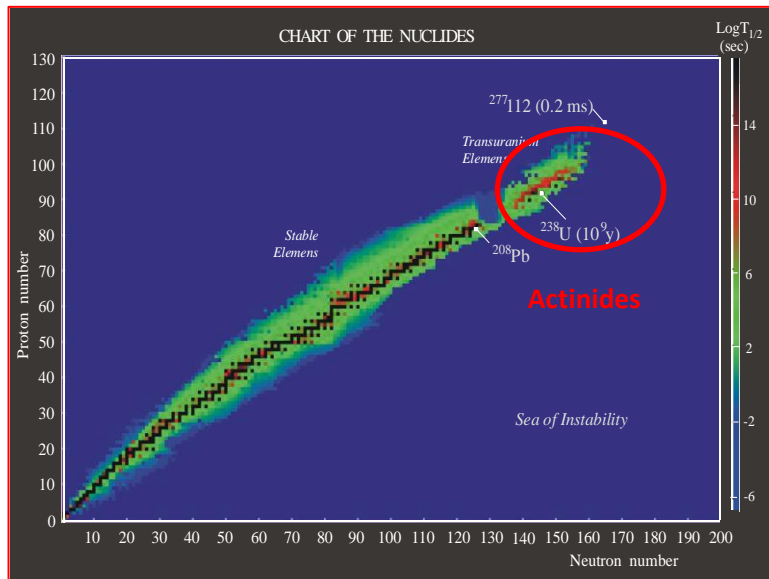
Discovering fission Otto Hahn proved the existence of Ba in U-samples irradiated by neutrons. From fission of Uranium the complement to Ba with $Z = 56$ is Kr with $Z = 36$. This asymmetry in charge or mass splits was later shown to be a general feature in the actinides, both for (n, f) reactions and spontaneous fission



The asymmetric mass split in (n, f) reactions induced by thermal neutrons in ^{2309}Th to ^{254}Es has two remarkable features:

1) For all reactions yield starts to rise in the heavy mass group at $A_H \approx 130$ u. The corresponding charge is the magic $Z = 50$. The mass center of the heavy group stays \approx constant, the mass center of the light group follows the increase of compound mass.

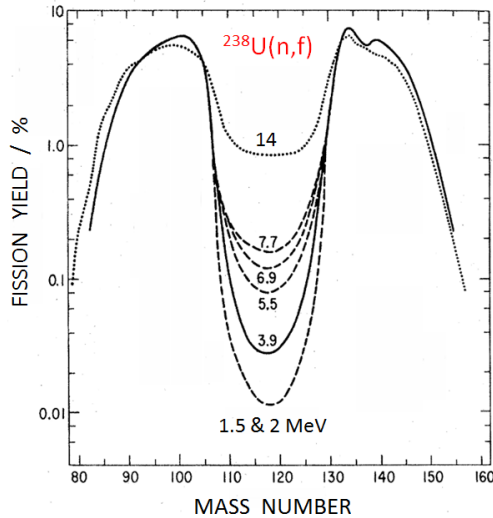
2) The mass yield curve exhibits a fine structure. It appears to be linked to even charge splits for the compound nuclei Th-Cf with even compound charge $Z = 90 - 98$.



Chap. II

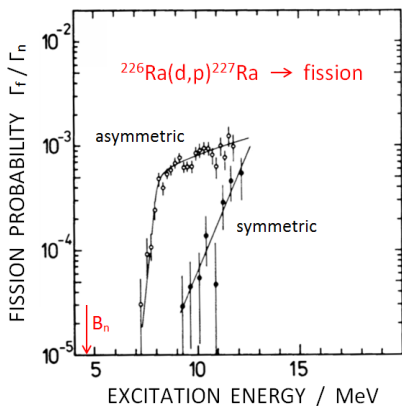
Symmetric versus Asymmetric Fission

In (n,f) reactions the mass yield near symmetric mass splits rises rapidly with the increase of the energy E_n of neutrons inducing fission. The contribution of symmetric fission comes



Nagy 1978

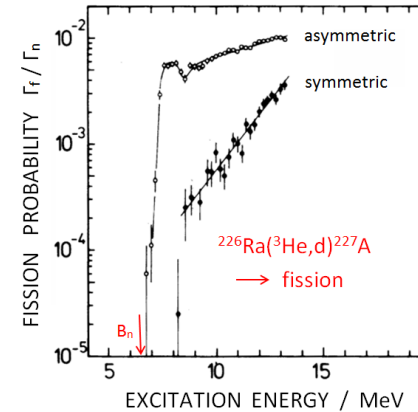
into view in a logarithmic plot. For $^{238}\text{U}(n,f)$ the symmetric yield rises by two orders of magnitude for E_n from 1.5 to 14 MeV.



In the (d,p) reaction for ^{226}Ra , simulating absorption of a neutron, fission probabilities could be determined separately for symmetric and asymmetric fission of ^{226}Ra . For the two processes the thresholds are shifted by ≈ 2 MeV.

Konecny 1974

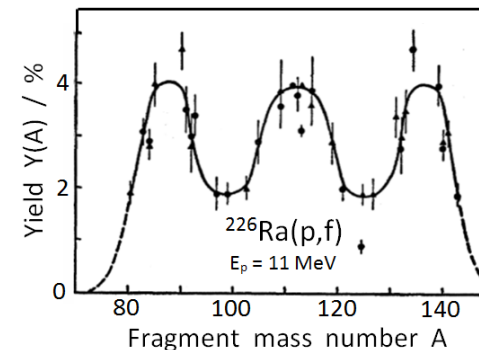
A similar observation as for the (d,p) reaction on ^{226}Ra is reported for the $(^3\text{He},d)$ reaction. Instead of a neutron a



proton is absorbed. The fissioning nucleus is ^{226}Ac . A similar observation as in fission of ^{226}Ra is made: the threshold for symmetric fission is higher by $\approx 1,5$ MeV compared to asymmetric fission.

Konecny 1974

The same reaction was studied more directly in proton induced fission of ^{226}Ra for incoming proton energies of 11 MeV. This corresponds to an excitation energy of ≈ 15 MeV.

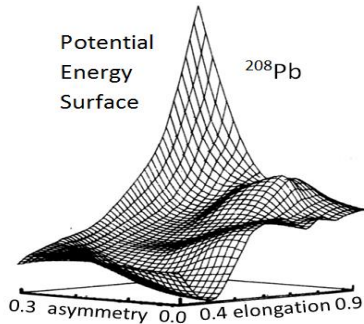


At this excitation energy the yields for symmetric and asymmetric fission have become equal. The mass distribution is triple-humped.

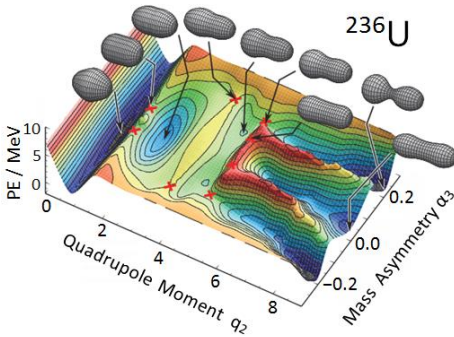
Jensen 1958

The above experiments suggest that symmetric and asymmetric fission are two different modes of fission. This led already in 1951 to the Two-Mode Hypothesis by Turkevich – Niday. The hypothesis has found an explanation in the study of potential energy surfaces of nuclei near the fission barrier.

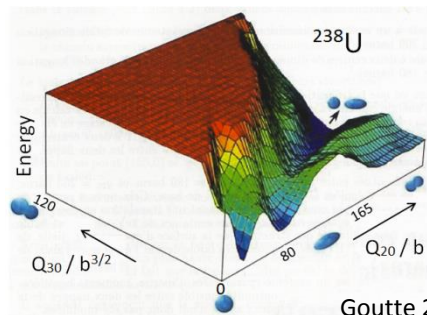
For the discussion of mass distributions the Two-Mode Hypothesis suggests to consider symmetric and asymmetric fission as two distinct modes of fission. The idea is supported by calculations of the potential energy surface near the saddle point. A sample of results from shell-corrected LDM theories



Pashkevich 1971



P. Möller 2009

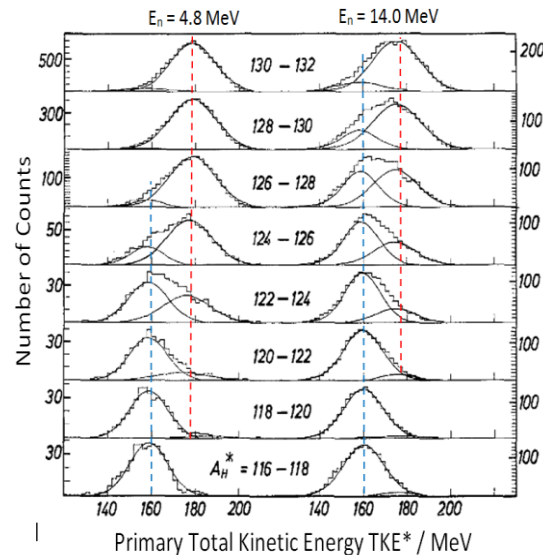


Goutte 2005

for ^{208}Pb and ^{236}U , and from microscopic HFB models for ^{238}U are on display. Comparing thresholds in the PES near the barriers they show that for Pb symmetric and for U asymmetric fission is favored.

Symmetric and asymmetric modes are seen to proceed along valleys towards scission. The two valleys are well separated by high ridges preventing a spill over from valley to valley. The two modes are in fact distinct and evolve independently. This is corroborated by experiment.

In the symmetric LDM mode no shell effects of fragments come into play while in the asymmetric mode the magic heavy fragment ^{132}Sn not only fixes the position of the heavy mass group but also favors more compact scission configurations. The kinetic energy of fragments is hence expected to be larger in the asymmetric mode than in the symmetric mode. The clean separation between the two modes becomes therefore better evident for mass distributions constrained by fragment kinetic energy. For $^{232}\text{Th}(n,f)$ the symmetric mode starts at symmetry with $\text{TKE} = 160 \text{ MeV}$ and TKE stays about constant until the mode tapers off when moving towards mass asymmetry. The asymmetric mode comes into view already close to symmetric fission albeit at very small yield and in any case with TKE shifted to larger energies by some 20 MeV.

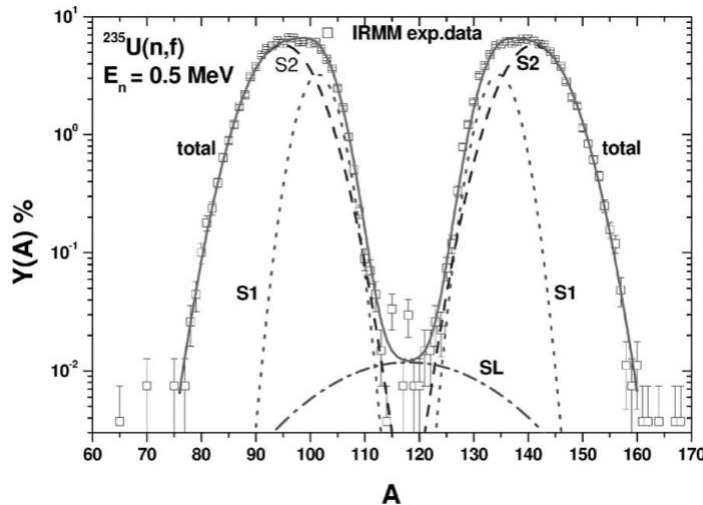


Pfeiffer 1970

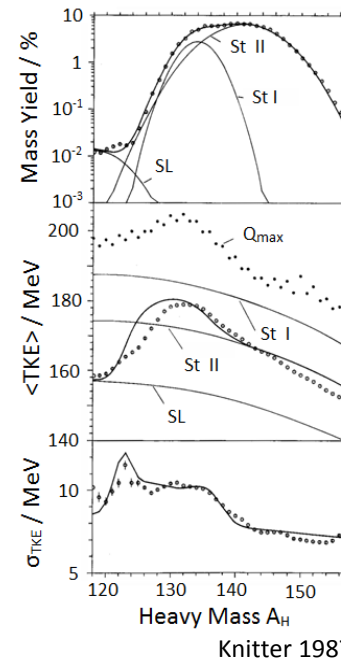
In mass regions where one of the modes is prevailing the distribution of TKE is well described by Gaussians. In the mass ranges of mode overlap TKE is skewed. The example is for $^{232}\text{Th}(n,f)$ at two neutron energies 4.8 and 14.0 MeV.

In the detailed analysis of many fission reactions it turned out that a satisfactory description of mass and energy distributions requires the introduction of more than one mass asymmetric mode. By theory this was proposed in the Brosa-Grossmann-Müller model of scission. The modes called for short the Brosa modes are the superlong symmetric mode (SL) and two asymmetric modes standard I and standard II (St I and St II). The bifurcation of the asymmetric mode into St I and St II occurs once the asymmetric saddle point has been passed. The position of the mode St I is centered at the heavy mass $A_H \approx 135$ while for the mode St II the center is at $A_H \approx 142$. It is therefore conjectured that St I is steered by the doubly magic ^{132}Sn and St II by the deformed neutron shell with $N = 88$. Note that for all three modes the mass distribution is assumed to be Gaussian in shape.

In the example shown for the reaction $^{235}\text{U}(n,f)$ the fit is seen to be very satisfactory.



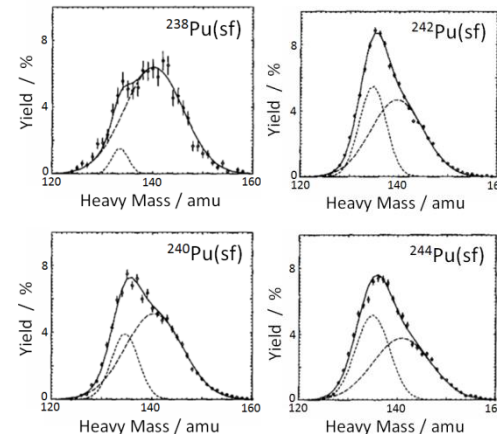
Hambusch 2003



Knitter 1987

The combined analysis of mass and TKE distributions for $^{235}\text{U}(n,f)$ in terms of modes is convincing. Not only the mass distribution but also properties of the total kinetic energy TKE are consistently parameterized. The average $\langle \text{TKE} \rangle$ as a function of mass A is seen to come about as a superposition of the three modes with each mode having its own characteristic TKE depending on mass. The weights of the modes are obtained from the fit to the mass distribution. Remarkably the variance σ_{TKE} of the $\text{TKE}(A)$ distributions exhibits bumps at the overlap of modes.

In the mass distributions of Pu-isotopes undergoing spontaneous fission a striking variation in the shape of the mass distributions is reported. In the decomposition of mass



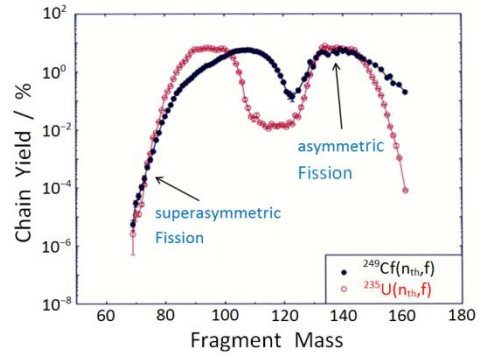
yield into the modes St I and St II it appears that the variation in shape should be attributed to varying weights of the two modes. Surprisingly the relative weights of the modes St I and II change suddenly from isotope to isotope.

Demattè 1997

Chap. II

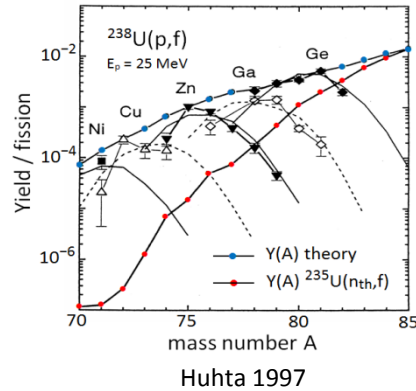
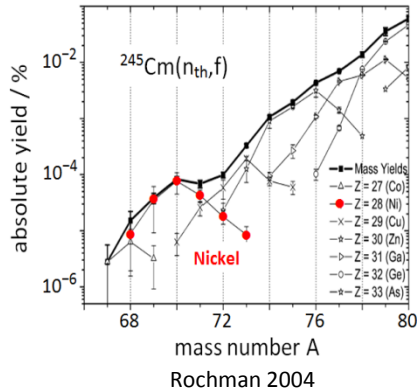
Supersymmetric Fission

Exploring fragment mass distributions at very asymmetric splits of the fissioning nucleus a new phenomenon emerges. Comparing the mass distributions for $^{235}\text{U}(n_{\text{th}},f)$ and $^{249}\text{Cf}(n_{\text{th}},f)$



it is noticed that there are two mass regions where yields become virtually identical. Besides modes St I and St II stabilizing the asymmetric heavy peak by shell effects there exists at light masses near 70-80 amu a further A-range where yields are

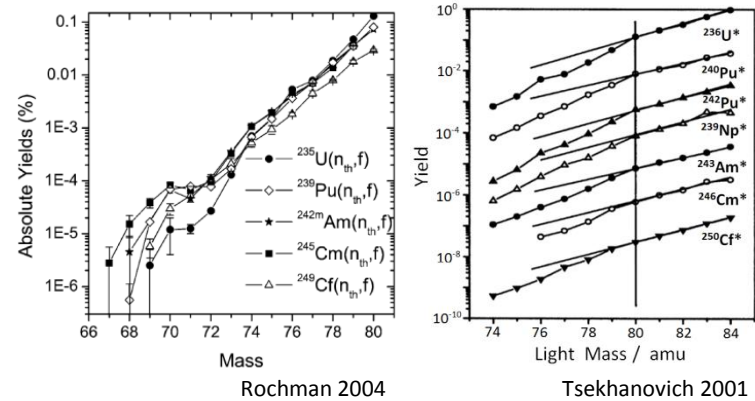
identical. This is attributed to the presence of shells with $Z = 28$ and $N = 50$ in the light fragment.



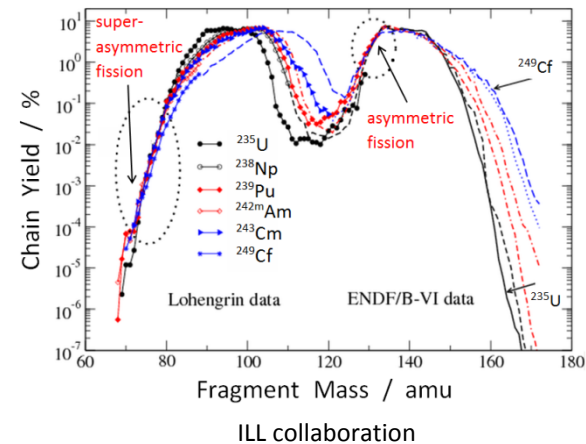
Supersymmetric fission in (n_{th},f) of ^{245}Cm becomes manifest as a bump near $A = 70$ attributed to the high yield of ^{70}Ni with $Z = 28$ (Fig. to the left).

At higher excitation energies the yield of super-asymmetric fission may increase by orders of magnitude compared to thermal neutron fission. This is e.g. observed for the reaction $^{238}\text{U}(p,f)$ at a proton energy of 28 MEV (Fig. to the right).

The bump structure near $A = 70$ has been found for all (n_{th},f) reactions studied on the LOHENGRIN mass separator (Fig. to the left). Less spectacular is a kink at mass $A = 80$ in the slope of the mass distributions. Tentatively one may trace it to the stabilizing effect of ^{82}Ge with $N = 50$ which after evaporation of 2 neutrons is observed as ^{80}Ge (Fig. to the right).



Summarizing, all (n_{th},f) reactions in the actinides undergoing with thermal neutrons asymmetric fission also exhibit as a common feature supersymmetric fission.



Velocities and Kinetic Energies of Fragments

The energy available in n-induced fission is the Q-value:

$$Q^* = M_{\text{target}} + M_{\text{neutron}} + E_{\text{neutron}} - (M_L^* + M_H^*)$$

It is shared between total kinetic and excitation energy TKE* and TXE, respectively, of primary fragments

$$Q^* = \text{TKE}^* + \text{TXE}.$$

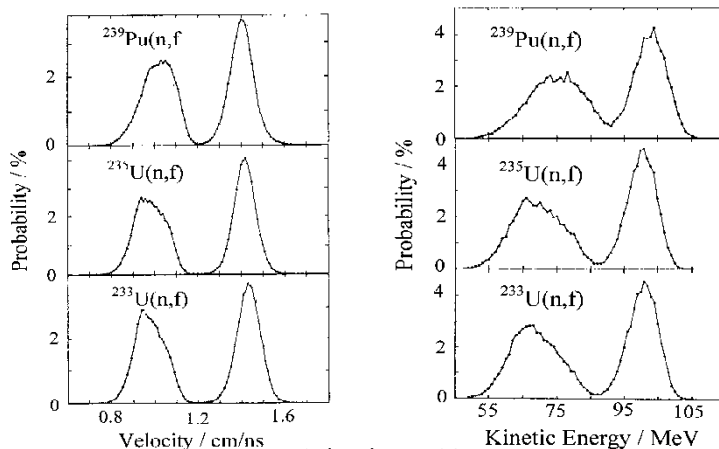
To the total kinetic energy TKE* contribute both the light and the heavy fragment with their kinetic energies E_L^* and E_H^* :

$$\text{TKE}^* = E_L^* + E_H^* = (k/2)M_{\text{CN}}V_L^*V_H^*.$$

The total kinetic energy release is found by measuring fragment velocities V_L^* and V_H^* for given compound mass M_{CN} of the fissioning nucleus. The factor $k = 1.0365$ keeps track of the transformation of units to those in use in nuclear physics, viz. amu for masses M , (cm/s) for velocities and MeV for energies.

In the CM system of fragments the momenta \mathbf{p}_L^* and \mathbf{p}_H^* of primary fragments cancel each other. The absolute values are equal: $M_L^*V_L^* = M_H^*V_H^*$ whence $M_L^*/M_H^* = E_H^*/E_L^*$

For the three standard reactions in thermal neutron fission ^{233}U , ^{235}U and ^{239}Pu the distributions of velocities $P(V^*)$ and kinetic energies $P(E^*)$ are compared in the figure.



Geltenbort 1985

Evidently the two bumps to the left and right in the velocities and energies reflect the heavy and light mass group of fragments. Note that on average the velocity and energy for the light group is larger than for the heavy group. Average velocities in cm/s, masses in amu and energies for the L and H group in MeV for the reaction $^{235}\text{U}(n_{\text{th}},f)$ are given in the table:

$\langle V_L^* \rangle$	$\langle V_H^* \rangle$	$\langle M_L^* \rangle$	$\langle M_H^* \rangle$	$\langle E_{\text{KL}}^* \rangle$	$\langle E_{\text{KH}}^* \rangle$
1.420(5)	0.983(5)	96.4(2)	139.6(2)	100.6(5)	69.8(5)

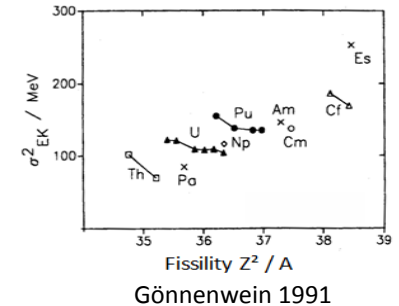
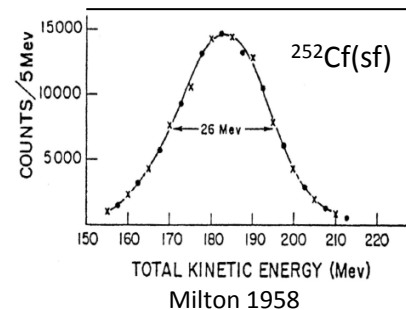
In the following table average total kinetic energies $\langle \text{TKE}^* \rangle$ for thermal neutron and spontaneous fission are summarized

Reaction	$^{233}\text{U}(n,f)$	$^{235}\text{U}(n,f)$	$^{239}\text{Pu}(n,f)$	$^{252}\text{Cf}(sf)$
TKE*/MeV	170.1(5)	170.5(5)	177.9(5)	184.0(13)

From the table it emerges that the energy release increases with the mass or charge of the fissioning nucleus. From a fit to experimental data Viola proposed a dependence on the Coulomb parameter $Z^2/A^{1/2}$. The approach is very successful:

$$\langle \text{TKE}^* \rangle = 0.1189(11) Z^2/A^{1/2} + 7.30(15) \text{ MeV}$$

Besides the average also the distribution of TKE* is of interest. Example: for $^{252}\text{Cf}(sf)$ it is Gaussian-like (left figure). In the right figure the width of the distribution as described by the variance σ^2_{EK} is seen to increase with fissility Z^2/A .

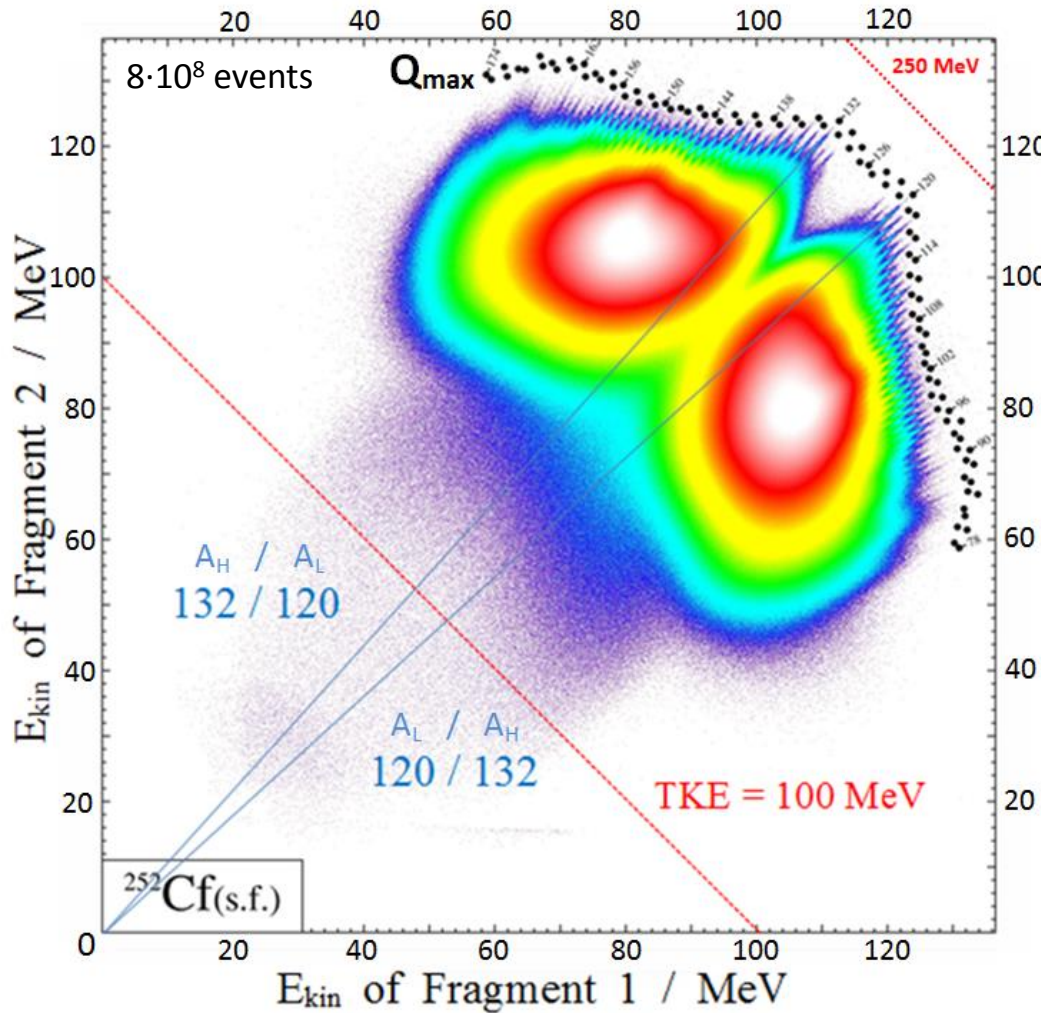


Milton 1958

Gönnenwein 1991

Chap. III

The 2V- and 2E-methods to measure mass distributions



A. Möller 1995

Based on momentum conservation

$$M_L^* V_L^* = M_H^* V_H^*$$

and mass conservation

$$M_L^* + M_H^* = M_{CN}$$

fragment masses are found in 2V- experiments as

$$M_L^* = M_{CN} [V_H^* / (V_H^* + V_L^*)].$$

More common are 2E-experiments.

$$\begin{aligned} \text{Since } E_L^* / E_H^* &= \frac{1}{2} M_L^* V_L^{*2} / \frac{1}{2} M_H^* V_H^{*2} \\ &= V_L^* / V_H^* \end{aligned}$$

similar relations hold in 2V- and 2E-experiments:

$$\begin{aligned} M_L^* E_L^* &= M_H^* E_H^* \\ M_L^* &= M_{CN} [E_H^* / (E_H^* + E_L^*)] \end{aligned}$$

NOTE: the asterisk* labels quantities before neutron evaporation. Hence, in a 2V- or 2E-scatter plot sharp mass lines are only observed for neutronless fission (cold fission) at the highest TKE coming close to the Q-value. When at lower TKE neutron evaporation is setting in, the mass lines get mixed and the line structure is blurred.

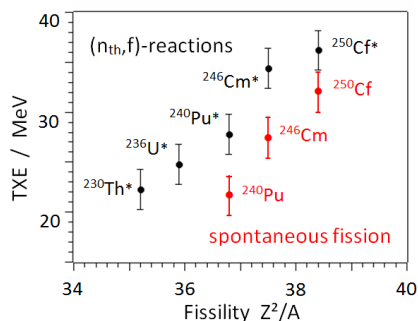
In principle the total excitation energy TXE could be found from energy conservation as

$$TXE = Q^* - TKE^*$$

However, to calculate Q^* not only the primary mass distributions $Y(A^*)$ but more in detail the yields $Y(A^*, Z)$ have to be known. This is unfortunately not the case and therefore TXE has to be found by adding its contributions to n and γ emission:

$$TXE = v_{tot} \cdot [B_n + \eta] + E_{\gamma tot}$$

with v_{tot} the total neutron multiplicity, B_n the neutron binding energy, η the neutron kinetic energy in the CM of fragments and $E_{\gamma tot}$ the total prompt gamma energy. The average total excitation energy $\langle TXE \rangle$ calculated for thermal neutron and spontaneous fission in a range of actinides is presented in the figure.



There is a clear correlation between the excitation energy $\langle TXE \rangle$ and the fissility parameter Z^2/A . The increase of $\langle TXE \rangle$ with fissility follows the increasing neutron emission for heavier nuclei.

As a rule, in spontaneous fission average excitation energies $\langle TXE \rangle$ are smaller than in thermal neutron fission. This may be attributed to the smaller potential energy gain ΔV from the exit point of the barrier down to scission in spontaneous fission.

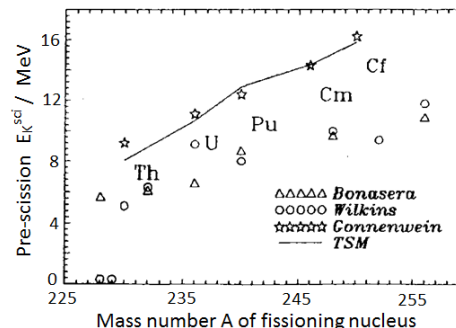
Both energies TKE* and TXE are already present at the scission point with a certain fraction. However, major contributions are at scission still bound as potential energies V_{Coul} and V_{def} , respectively. Formally

$$TKE^* = E_K^{sci} + V_{Coul} \quad \text{and} \quad TXE = E_X^{sci} + V_{def}$$

V_{Coul} is the energy of mutual Coulomb interaction between fragments, and V_{def} the deformation energy of the two fragments at the scission point. The energies at scission E_K^{sci} and E_X^{sci} not bound as potential energies are fed by the gain in potential energy ΔV in the descent from saddle to scission and the excitation energy of the compound nucleus E_{CN}^* left at the barrier B_f :

$$E_K^{sci} + E_X^{sci} = \Delta V + (E_{CN}^* - B_f)$$

The share of E_K^{sci} and E_X^{sci} in the potential energy gain ΔV is discussed controversially. It depends on the viscosity of the flow of nuclear matter from saddle to scission. Is the flow honey- or water-like? In experiment the dissipated energy E_X^{sci} has been estimated from the charge even-odd effect of fragments. Combined with theoretical models for the energy gain ΔV the pre-scission kinetic energy E_K^{sci} is derived albeit with large uncertainties as $E_K^{sci} = \Delta V - E_X^{sci}$.

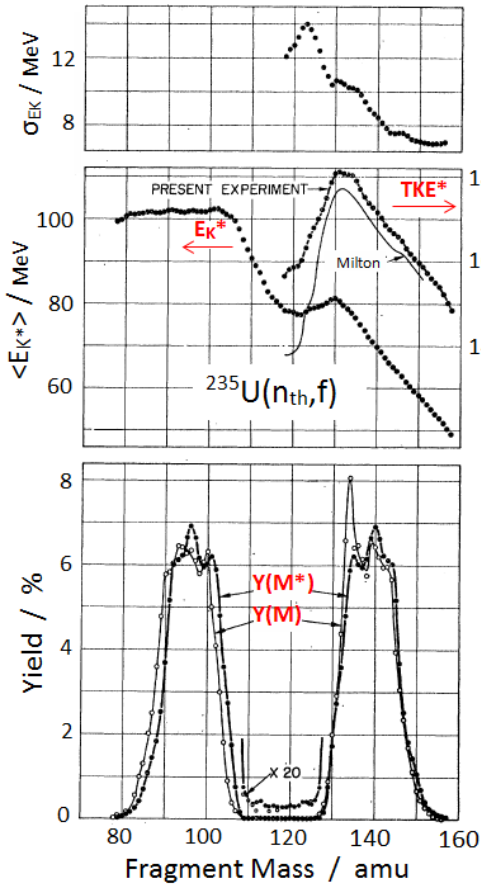


In the figure the stars depict E_K^{sci} obtained. The through-going line is a fit to the data in a Two-Spheroid-Model. The other points are from different purely theoretical models.

Chap. III

Mass-Energy Correlations

Mass-energy correlations of fragments were investigated in a series of classic papers setting standards. The main reactions being of importance for applications were studied in the sixties of last century with the newly developed surface barrier detectors. Mass distributions before and after prompt neutron emission $Y(M^*)$ and $Y(M)$, respectively, average energies of



H.W. Schmitt 1966

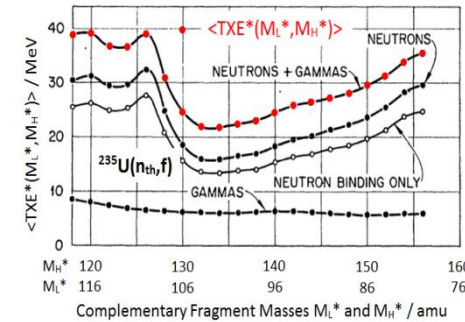
single fragments $E_K^*(M^*)$, total average energies $TKE^*(M^*)$ and the variance $\sigma_{EK}(M^*)$ of energy distributions were surveyed.

Notable facts:

- $Y(M^*)$ has more fine structure than $Y(M)$
- Light fragments have larger energies than the heavy ones
- TKE^* peaks at $M = 132$
- for symmetric fission there is a dip in TKE^*
- the variance has structure when modes overlap (see foil A06)

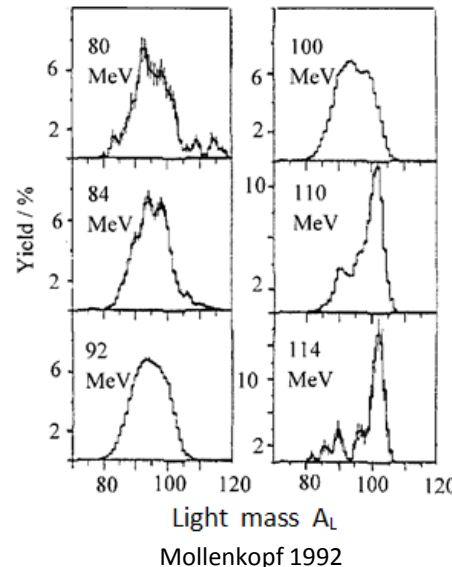
Results shown here for fission of ^{235}U by thermal neutrons are similar for $^{233}\text{U}(n,f)$ and $^{239}\text{Pu}(n,f)$, and spontaneous fission of ^{252}Cf .

With Q-values calculated from mass tables and kinetic energies of fragments measured, the average total excitation energies $\langle TXE(M_H^*, M_L^*) \rangle$ may be found for any mass split (M_L^*, M_H^*) . They are plotted in the figure as red points for the reaction $^{235}\text{U}(n_{th}, f)$. The excitation energies are particularly large near symmetric mass splits thus compensating the dip in kinetic energy TKE^* . In the figure the energy is further decomposed into the contributions by neutrons and gammas.



H.W. Schmitt 1966

Mass distributions taken in a window of kinetic energy $E_L(M)$ of fragments exhibit a fine structure varying with energy. A sample of mass distributions within energy windows of 4 MeV in width for the light group in $^{235}\text{U}(n,f)$ are Gaussian-like only for energies near the average. Both at very high and at very low energies a fine structure appears with peaks about 5 mass units apart. The phenomenon has been scrutinized in connection with fragment charge even-odd effects in cold fission.



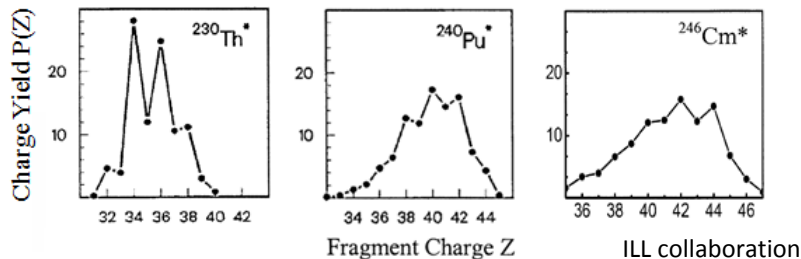
Mollenkopf 1992

Asymmetric Fission

Charge distributions of fission fragments closely follow the mass distributions. The ratio of fragment charge numbers to mass numbers Z_{FF}/A_{FF} is to first approximation identical to the corresponding ratio Z_{CN}/A_{CN} of the fissioning compound nucleus. There are only slight deviations from this UCD rule of "unchanged charge density". Note that $Z_L + Z_H = Z_{CN}$.

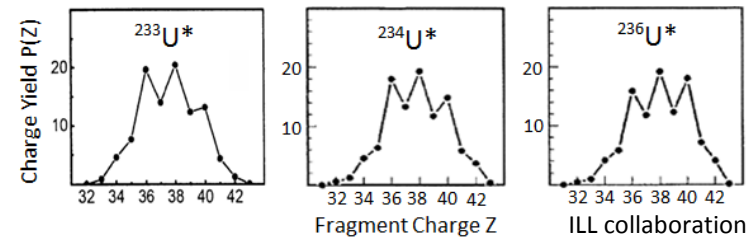
However, in particular in low energy fission of actinides, there is a pronounced staggering of charge yields $Y(Z)$ in case of even- Z fissioning compounds. The phenomenon has been scrutinized by radiochemical and physical methods for reactions ranging from (sf), (n,f), (γ ,f) ... to fission by Coulomb excitation. In the following mainly n-induced fission is considered.

Comprehensive studies were performed at the Institut Laue-Langevin for the (n,f) reaction with thermal neutrons for targets from ^{229}Th to ^{249}Cf . A sample of charge distributions measured for even- Z compounds is shown in the figure. Only results for



the light fragment group are given. For e- Z compounds the charges in the heavy group are strictly identical to those in the light group mirrored at symmetry. Since upon approaching symmetric fission the charge yields in the figure are seen to fade away the full charge distributions are like the mass distributions asymmetric.

Catching the eye in the figure is the strong even-odd fluctuation in the charge yields. Systematically even fragment charges are favored compared to odd ones. The effect is most noticeable in the light actinide Th and nearly vanishes for the heavier actinide Cm. The question then is whether this tendency has to be attributed to the increase of compound mass A_{CN} , or compound charge Z_{CN} , or fissility Z_{CN}^2/A_{CN} , or any other parameter. Having been suggested.



An answer to this question may be found by inspecting charge distributions at fixed charge Z_{CN} . This is done in the figure for three U-isotopes with $Z_{CN} = 92$. The staggering is observed to stay pretty constant. It is hence concluded that the e-o staggering depends crucially on compound charge Z_{CN} . The compound neutron number N_{CN} or mass number A_{CN} does not appear to influence the effect.

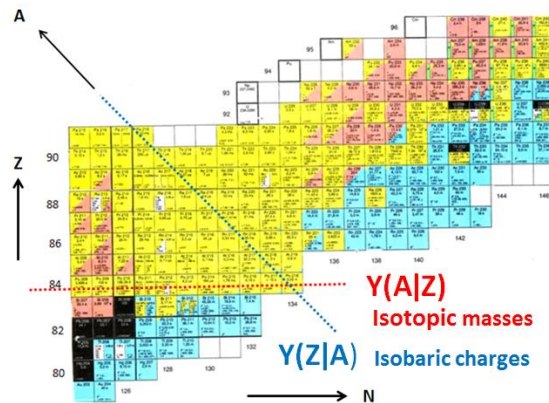
The even-odd staggering was also analyzed for neutrons. There is however a difficulty due to the evaporation of neutrons from the fragments. A strict conservation law $N_{LF}^* + N_{HF}^* = N_{CN}$ is only valid for primary fragments before neutron emission. Yet, the measurement of primary masses A_{FF}^* and charges Z_{FF} is in actual practice not feasible. Reliable results were only obtained in rare cold fission where there is no neutron evaporation at all.

Chap. IV

Conditional Distributions

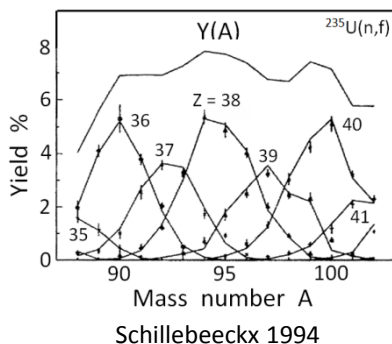
Knowing masses and charges of fission fragments allows for a more detailed insight into the distributions of fragments. Two types of conditional distributions may be evaluated:

isotopic mass distributions : $Y(A|Z)$
and isobaric charge distribution: $Y(Z|A)$



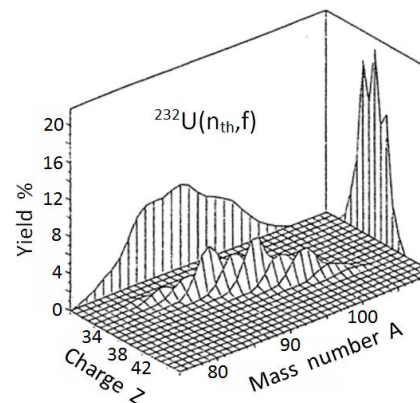
How these distributions come about is visualized in a zoom of the nuclide chart.

For the reaction $^{235}\text{U}(n,f)$ with thermal neutrons the individual isotopic mass distributions $Y(A|Z)$ together with their sum, the mass distribution $Y(A)$, are plotted for the light fragment group. Evidently the large yields of isotopic mass distributions for even fragment charges Z_L bring about a fine



structure in the mass yield curve $Y(A)$. Already in foil A03 it was pointed to this fine structure. The bumps in the mass yield are about 5 amu apart just corresponding to a step of two charges. Note that for ^{236}U the ratio $5/2$ is close $A_{CN}/Z_{CN} = 2.56$.

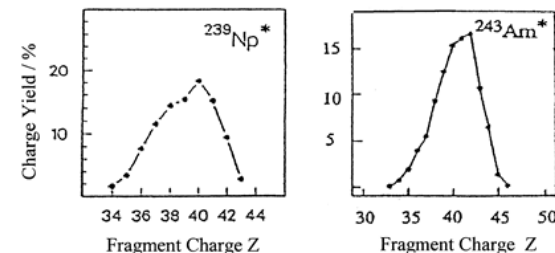
The relation between the sequence of isotopic mass distributions in a (A,Z) plane and their projections along mass or charge yielding mass and charge distributions is brought out in a 3-dim plot. The data are for $^{232}\text{U}(n_{th},f)$. The plot makes understandable how a strong fluctuation in charge yields leads to a rather gentle modulation in the mass yields.



Gönnenwein 1992

Charge Distributions from odd- Z_{CN} Compounds

Starting from the idea that the e-o staggering of charge yields in fission of even- Z_{CN} compound nuclei is a reminiscence of the superfluid fully paired ground state of e-Z nuclei, it was conjectured that for odd- Z_{CN} nuclei with an unpaired proton any e-o fluctuation in charge yields should be absent. For the odd- Z_{CN} nuclei Np and Am this was indeed observed in standard asymmetric fission (see the figure). However, surprises came when moving to super-asymmetric fission.



ILL collaboration

Charge even-odd Effect

To quantitatively assess the fluctuations of charge yields in fission the even-odd effect δ_z is introduced with the definition

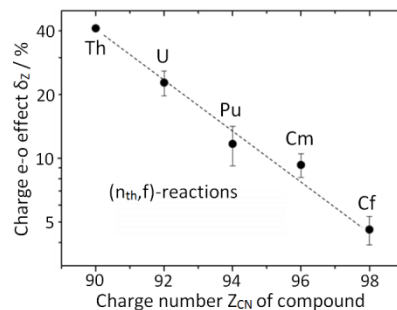
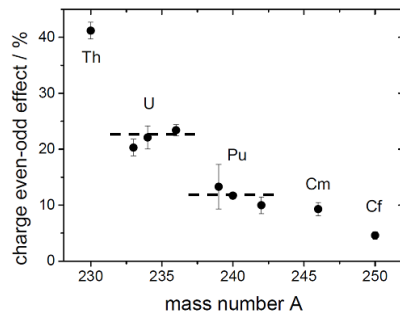
$$\delta_z = (Y_e - Y_o) / (Y_e + Y_o).$$

In this definition Y_e and Y_o are the sum of yields for even and odd charges, respectively. It is common use to normalize the sum to $(Y_e + Y_o) = 100$ and to quote the e-o effect δ_z in %.

In the table e-o effects for thermal neutron fission have been collected. Except for $^{238}\text{Pu}^*$ studied by radiochemistry, the data were obtained by physical methods at the ILL. The obvious

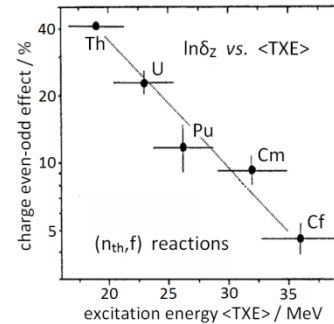
Nucleus	$^{230}\text{Th}^*$	$^{233}\text{U}^*$	$^{234}\text{U}^*$	$^{236}\text{U}^*$	$^{239}\text{Pu}^*$	$^{240}\text{Pu}^*$	$^{242}\text{Pu}^*$	$^{246}\text{Cm}^*$	$^{250}\text{Cf}^*$
δ_z / %	41.2(10)	20.3(15)	22.1(21)	23.4(10)	13.3(40)	11.7(5)	10.0(15)	9.3(12)	4.6(7)

decrease of the e-o effect was already addressed in foil Z01. There it was also argued that the effect essentially depends on the compound charge Z_{CN} , but not on compound mass A_{CN} . This is brought to evidence in two figures for δ_z as a function of compound mass and compound charge. For the three U- and the



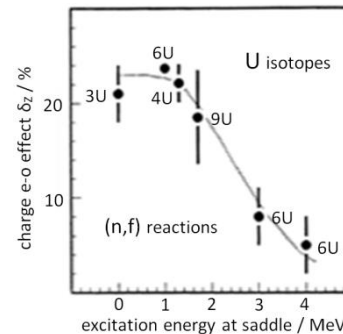
three Pu-isotopes the e-o effect is constant telling that the effect does not depend on the neutron number N_{CN} of the compound. By contrast, plotted logarithmically versus compound charge Z_{CN} the e-o effect δ_z is a smooth linear function sloping down for increasing charge.

There is an interesting interpretation of the charge e-o effect. In thermal neutron fission of fissile nuclei the nucleus is cold and hence fully paired at the saddle. The appearance of odd fragment charges indicates that in the process of fission proton pairs are broken. The energy required has to be provided by the excitation energy E_X^{SCI} the nucleus is gaining in the



descent from saddle to scission. The more excitation energy is available, the more pairs may be broken and the more the e-o effect is washed out. A first hint to support this idea is found in a plot of δ_z vs. total TXE. shown in the figure. A clear correlation is revealed. However, since $\text{TXE} = E_X^{SCI} + V_{\text{def}}$ it is not evident that the correlation is really due to E_X^{SCI} . Yet precisely this correlation is postulated in a model discussed below.

A cleaner argument is provided from a study of the charge e-o effect for the compound $^{236}\text{U}^*$ at different excitation energies above the saddle. Any excitation at saddle will go into excitation at scission. As shown in



the figure, experiment clearly demonstrates the dependence of the charge e-o effect on the excitation at saddle and hence at scission. The charge e-o effect is hence a sensitive detector of excitation energy E_X^{SCI} at scission.

Chap. IV

 δ_Z as a measure for E_X^{SCI}

For the even-odd effect δ_Z observed in fission of even Z_{CN} compound nuclei several theories have been developed. It is remarked that for near-barrier fission the fissioning compound is superfluid at the saddle with all protons and neutrons being paired. The e-o effect $0 < \delta_Z < 1$ signals the presence of odd numbers of protons in the fragments. It must come about by quasi-particle excitations breaking proton pairs in the course of fission from saddle to scission provided the two single protons from a pair are going to complementary fragments. The mechanism of pair-breaking is left open.

Formally the following quantities are introduced:

N_{max} = maximum number of q-p excitations available

depending on excitation energy E_X^{sci} at scission

q = probability to break a pair when the energy is available

ϵ = probability for broken pair to be a proton pair

p = probability for nucleons from a broken pair to go into complementary fragments.

With the normalization of charge yields $(Y_e + Y_o) = 1$ the e-o effect $\delta_Z = (Y_e - Y_o) / (Y_e + Y_o)$ becomes

$$\delta_Z = (1 - 2Y_o).$$

If at most one pair only can be broken ($N_{max} = 1$) the odd charge yield Y_o of fragments is $Y_o = q\epsilon p$. Hence $\delta_Z = (1 - 2q\epsilon p)$. For $N_{max} > 1$

$$\delta_Z = (1 - 2q\epsilon p)^{N_{max}}.$$

On the other hand the energy consumed is given by the average number $\langle N \rangle$ of broken pairs with the energy 2Δ required to create 2 q-p excitations. Since $\langle N \rangle = qN_{max}$ the excitation energy at scission $E_X^{SCI} = 2\Delta \langle N \rangle$ is found to be

$$E_X^{SCI} = 2\Delta q N_{max}$$

Eliminating N_{max} from the two last equations yields the result

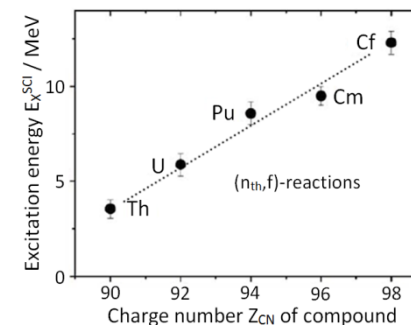
$$E_X^{SCI} = \frac{2\Delta q}{\ln(1 - 2q\epsilon p)} \ln \delta_Z$$

The model outlined describes in physical terms the way how perfect superfluidity for near-barrier fission at the saddle point, is partially destroyed in the fragments. The model predicts that the excitation energy at scission E_X^{SCI} is proportional to the logarithm of the e-o effect δ_Z .

The model does however not allow to give precise figures for the energy E_X^{SCI} since the only parameter known with certainty is $2\Delta = 1.7$ MeV at the saddle point. For the parameter ϵ a reasonable approximation is $\epsilon = Z_{CN}/A_{CN}$. But the choice for the parameters q and p is pure guess work. To first approximation both may be set as $q = 1/2$ and $p = 1/2$. With this choice one finds

$$E_X^{SCI} = -3.8 \ln \delta_Z$$

Since according to the model the excitation at scission E_X^{SCI} is proportional to the logarithm of the e-o effect $\ln \delta_Z$, and since δ_Z when plotted logarithmically decreases linearly with the compound charge number Z_{CN} , the energy drained up to scission from the potential energy gain ΔV



increases linearly with compound charge Z_{CN} . As visualized in the figure, for thermal neutron fission of the actinides Th to Cf the excitation energy increases from about 3 to 12 MeV. Other choices of the parameters, like $q = 1$

and $2\Delta = 2.4$ MeV for pair-breaking near scission are discussed. This leads to

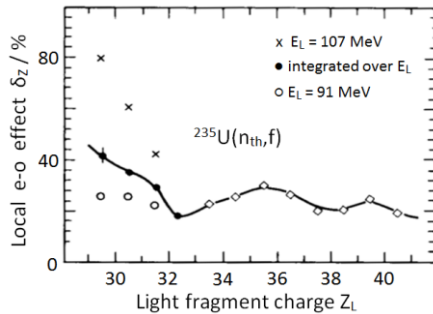
$$E_X^{SCI} = -2.3 \ln \delta_Z.$$

reproducing better the decrease of δ_Z when the excitation at the saddle point is raised (see preceding foil).

Even charge compound nuclei

Inspecting the charge distributions for even-Z compound nuclei it emerges that the eo-staggering is not constant over the full range of charges. This has been the motivation for introducing the notion of local eo-effects. Various prescriptions how to assess this local eo-effect have been proposed.

The local eo-effect in particular highlights the rise of the eo-staggering of fragment charge yields in supersymmetric fission. This is visualized in the figure for $^{235}\text{U}(n_{th},f)$ integrated over LF kinetic energy E_L and for two fixed E_L . The effect steeply rises for large E_L and hence low excitation energy. The analysis explores

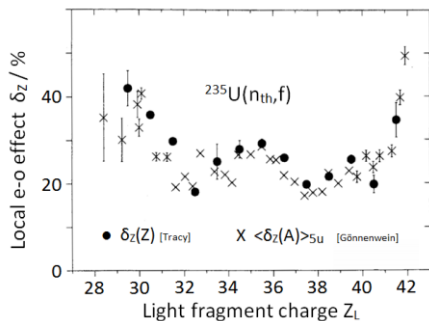


Sida 89

deviations from an overall Gaussian charge distribution.

The physical reason for the surge of eo-effects is thought to be due to the shell effect in the light fragment. Magic fragments are not likely to pick up protons from a broken pair.

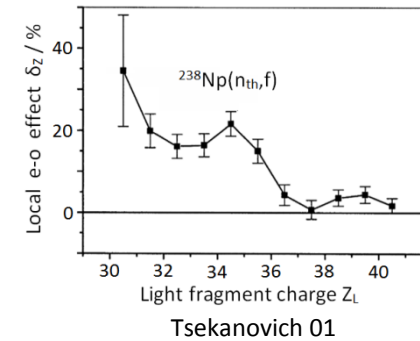
For this conjecture to be valid a similar rise of the eo-staggering should also be observed close to the magic heavy fragment with $Z_H = 50$. This appears to be the case for $^{233}\text{U}(n_{th},f)$ where in the figure two different eo-effect evaluations come to the result that for $Z_L = 42$ and hence $Z_H = 50$ eo-effects are pronounced.



Gönnenwein 92

Odd charge compound nuclei

As already outlined above, in standard fission of compound nuclei with odd charge numbers Z_{CN} like Np with $Z_{CN} = 93$ there is no sizable eo-staggering. This was to be expected for a nucleus with an un-paired proton which is free to move to one or the other fragment. But when in



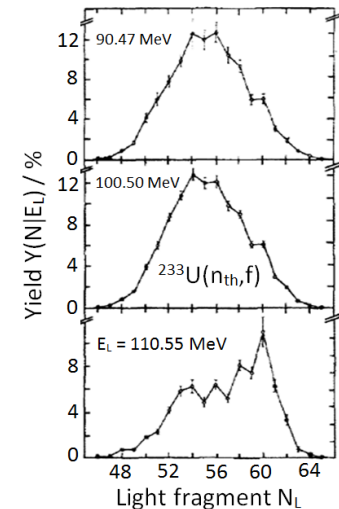
Tsekanovich 01

fission of nuclei with an even Z_{CN} the large eo-effects became known, the measurements were also pushed for odd Z_{CN} into these mass regions of low yield. As shown for $^{238}\text{Np}(n_{th},f)$ the same surge was found. This result corroborates the interpretation given that in supersymmetric fission magic fragments will not attract unpaired protons.

borates the interpretation given that in supersymmetric fission magic fragments will not attract unpaired protons.

Comment on δ_N :

To determine the eo-staggering of neutron numbers N^* before neutron evaporation is technically not feasible. All measured distributions $Y(N)$ are for secondary fragments. Any effect in the primary distributions $Y(N^*)$ is hence washed out. This is what is observed e.g. in the reaction $^{233}\text{U}(n_{th},f)$. Only close to n-less fission at large fragment kinetic energies E_L a small eo-effect δ_N appears.



Quade 88

Chap. V

Neutrons and Gammas

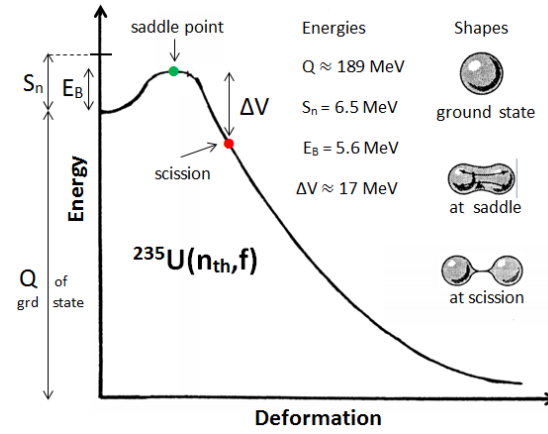
Energy balance in fission reads

$$Q^* = TKE^* + TXE$$

with Q^* the total available energy calculated from mass tables and TKE^* the total kinetic energy of fragment determined by experiment. Though the main part of the available energy Q^* is converted into kinetic energy TKE^* a sizable fraction of excitation energy TXE remains. Typical examples for the average excitation energy $\langle TXE \rangle$ are $\langle TXE \rangle \approx 24$ MeV for the reaction $^{235}\text{U}(n_{th}, f)$ and $\langle TXE \rangle \approx 36$ MeV for spontaneous fission of ^{252}Cf . This energy is evacuated by the emission of neutrons and gammas.

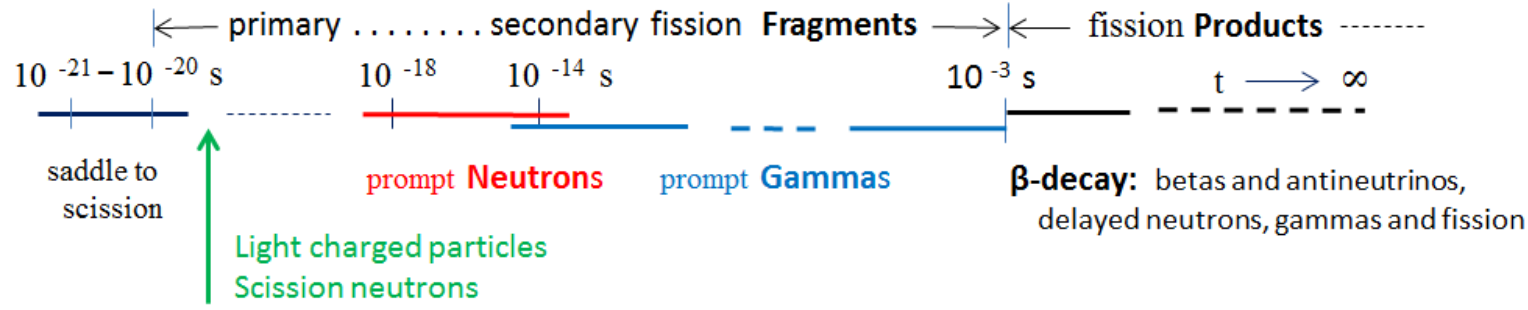
Since evaporation times for neutrons are much shorter than emission times for gammas, excited fragments first cool down by neutron emission. Following neutron emission by "primary fragments" (labelled by an asterisk) the nuclei are called "secondary fragments" or simply "products". When the remaining excitation has fallen below neutron binding energies the emission of gammas is setting in. The change-over from neutron to gamma emission is at about 10^{-14} s. Gamma emission may last up to 1 ms. Fission products have then reached their ground states. Yet they are still too n-rich and hence liable to β^- -decay. The decay times may be very long. The radioactivity of fission products is part of the activity of fuel remnants from nuclear power stations. The time scale of fragment de-excitation by neutrons and gammas is visualized in the figure.

Characteristic times in fission



- Time from grd state to saddle in low energy fi $6 \cdot 10^{-15}$ s
- Time from saddle to scission ≈ 5 zs
- Neck rupture in ≈ 0.5 zs
- Acceleration of FF to 90% of final velocity ≈ 5 zs
- Time for relaxation of deformation ≈ 5 zs
- Evaporation time for 10 MeV n from FF 10^3 zs

Once the saddle has been passed the fission process is very fast, while it takes comparatively a long time to evaporate a neutron. This justifies the assumption that the bulk of neutrons is emitted from fully accelerated fragments.



Neutron multiplicity ν_n

In low energy fission by far most neutrons are evaporated from fully accelerated fragments. They exhaust the main part of the excitation energy TXE of fragments. To TXE contribute the intrinsic excitation E_X^{sci} accumulated in the descent from saddle to scission and the energy stored as deformation energy V_{def} at scission but converted into intrinsic excitation once the deformation is relaxed after neck rupture:

$$TXE = E_X^{sci} + V_{def}$$

This energy is shared between neutrons and gammas:

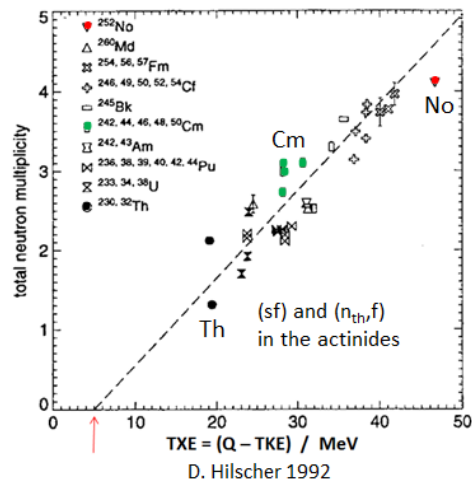
$$TXE = E_{ntot} + E_{\gamma tot}$$

with E_{ntot} and $E_{\gamma tot}$ the total neutron and gamma energies.

Neutron multiplicity ν_n is a key parameter of fission. It is defined as the number of neutrons emitted in one fission event. The table gives some examples for the average multiplicity $\langle \nu \rangle$ in thermal neutron fission.

CN nucleus	230Th	234U	236U	240Pu	246Cm	250Cf
$\langle \nu_{tot} \rangle$	2.08	2.50	2.43	2.89	3.83	4.08

Neutron multiplicity is a reliable measure of the energy



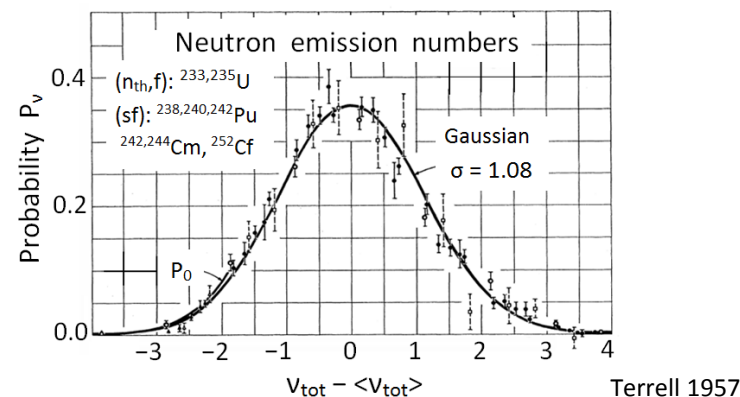
TXE = Q - TKE as demonstrated in the figure. A linear dependence of

ν versus TXE

is observed. The offset (red arrow on abscissa) marks the TXE not evacuated by neutrons but by gammas.

The **distribution of total neutron emission numbers** is in low-energy fission (spontaneous fission, thermal neutron induced fission) Gaussian-like, with centers at the average neutron multiplicity $\langle \nu \rangle$. Very early in the history of fission research it was remarked that the Gaussians are universal, i.e. identical for all low energy fission reactions (Terrell 1957). The standard deviation σ for all these reactions was given to be $\sigma = 1.08$.

$$P(\nu) = 0.36 \exp[-(\nu_{tot} - \langle \nu_{tot} \rangle)^2 / 2 \sigma^2] \quad \text{with } \sigma = 1.08$$



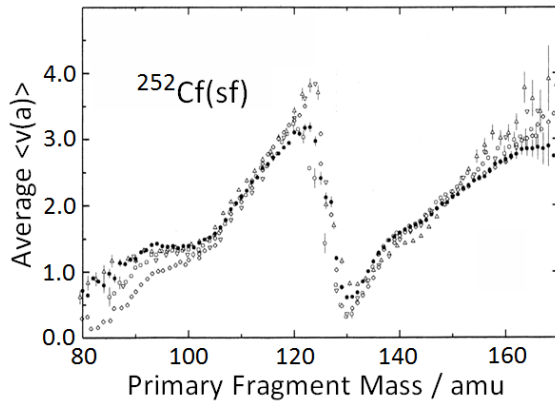
Nowadays it is established that the above rule for $P(\nu)$ is slightly oversimplified. Only for actinides from U to Cm the variance σ^2 is roughly constant with $\sigma^2 \approx 1.3$. For the actinides from Cf to No the variances rise significantly.

Of particular interest are the probabilities P_0 for neutron-less fission with $\nu = 0$. Compare the two characteristic reactions : (n_{th},f) of ^{235}U and (sf) of ^{252}Cf . The average multiplicities are $\langle \nu \rangle = 2.43$ and $\langle \nu \rangle = 3.76$, respectively. Though the averages $\langle \nu \rangle$ are close together, the probabilities for neutron-less fission P_0 differ by a factor of 14: $P_0 = 3.2\%$ and $P_0 = 0.23\%$, respectively.

The saw-tooth of neutron emission

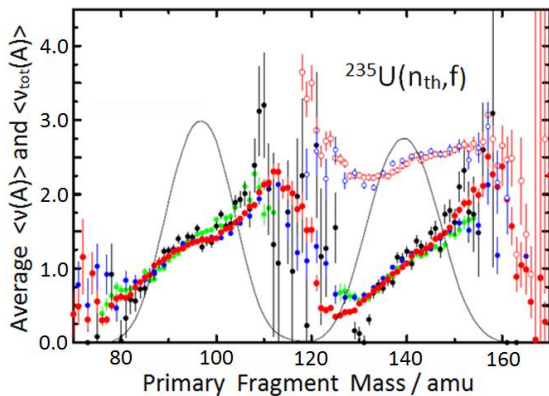
An important result from neutron studies in fission is the discovery that the neutron multiplicity has a peculiar dependence on fragment mass. Plotted as a function of fragment mass the average multiplicity $\langle v(A) \rangle$ has a saw-tooth like appearance. All experiments agree as to the general trends.

The neutron saw-tooth is best pronounced in low energy fission as demonstrated for $^{252}\text{Cf}(sf)$ and $^{235}\text{U}(n_{th},f)$ in the figures. Shown are the averages $\langle v(A) \rangle$ as a function of mass A.



A.S. Vorobyev 2001

- Vorobyev 2001
- △ Zakarova 1979
- Signarbieux 1972
- ▽ Walsh 1977
- Budtz-Jørgensen 1988



A.S. Vorobyev 2009

For $\langle v(A) \rangle$:

- Nishio 1998
- Maslin 1967
- Müller 1984
- Vorobyev 2009

For $\langle v_{tot}(A) \rangle$:

- Vorobyev 2009
- Maslin 1967

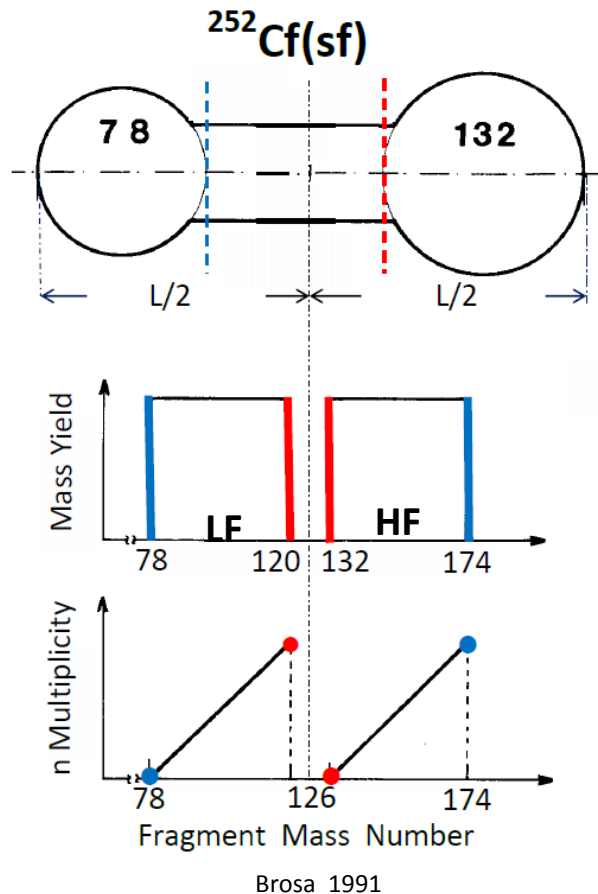
The saw-tooth phenomenon is intriguing. It is closely linked to the peculiarities observed in the mass-energy distributions of fragments. The minimum neutron multiplicity of $\langle v(A) \rangle$ for heavy fragment masses near $A = 130$ is the most startling phenomenon. It is a further evidence for stiff magic fragments close to ^{132}Sn remaining un-deformed at scission and hence carrying no deformation energy. All deformation energy is stored in the shape-distorted complementary light fragment. After shape relaxation the deformation energy is released by neutron evaporation leading to the peak of the saw-tooth $\langle v(A) \rangle$.

On average the light fragment group as a whole emits generally more neutrons than the heavy fragment group. Calling the group emission numbers v_L and v_H , respectively, some examples for v_L / v_H are collected in the table.

Reaction	$^{233}\text{U}(n_{th},f)$	$^{235}\text{U}(n_{th},f)$	$^{252}\text{Cf}(sf)$
v_L / v_H	1.395/1.100	1.390/1.047	2.056/1.710

As observed in the table, the light group emits about 20-30% more neutrons than the heavy group: $v_L / v_H \approx 1.2-1.3$.

The total neutron multiplicity $\langle v_{tot}(A) \rangle$ for a given mass fragmentation is found by summing the emission numbers $\langle v(A) \rangle$ of complementary fragments. The total multiplicity is seen in the figure for $^{235}\text{U}(n_{th},f)$ to peak at mass symmetry (open circles). Since the total available energy Q^* has to be shared between the kinetic and the excitation energy, $Q^* = \text{TKE}^* + \text{TXE}$, the peak in the total neutron emission, corresponding to a peak of excitation energy, just reflects a kinetic energy dip for fragments near symmetry. This energy dip of TKE is a well known phenomenon.



The study of fragment mass distributions in low energy fission of actinides has shown that in by far most cases the distributions are asymmetric: a fragment pair consists of a heavy and a light fragment. The mass asymmetry is attributed to the influence of shells in the nascent fragments. It is found that it is highly improbable to break up the spherical $Z=50$ and $N=82$ shells of fragments. This is concluded from the observation that nuclei near ^{132}Sn are the lightest nuclei with sizable yields in the heavy fragment group. Similarly, albeit less pronounced, the lightest fragments in the light fragment group are nuclei with masses around 78. This is traced to the spherical magic proton shell with $Z=28$ and the magic neutron shell with $N=50$.

In a very schematic model of nuclear fission the configuration at scission may hence be visualized like a dumb-bell consisting of two pre-fragments with masses 132 and 78 joined by a long neck (see top part of the figure). For the fissioning ^{252}Cf nucleus there remain 46 nucleons in the neck. To first approximation it is then assumed that the location where the neck is ruptured is distributed randomly along the neck. The stubs remaining after rupture are absorbed by the pre-fragments thereby establishing the final mass of the primary fragments observed in experiment. In the figure (middle part) the schematic mass distribution predicted by the model is on display. The distribution is asymmetric. The limiting mass ratios HF/LF are $132/120$ and $174/78$.

As a further consequence of the model the deformations of the primary fragments at scission are entirely due to the protruding stubs. The longer the stubs the larger will be the deformations. In the next step the stubs are absorbed by the pre-fragments and the deformation energy relaxes into intrinsic excitation of the fragments. The sharing of the deformation and hence excitation energy between the two fragments is asymmetric. For the mass ratio $\text{HF}/\text{LF} = 132/120$ all deformation and excitation energy goes to the light fragment, while for the ratio $174/78$ all excitation energy is found in the heavy fragment. Since the lion's share of the excitation energy is exhausted by neutron evaporation, the model predicts a saw-tooth behaviour of neutron multiplicity $\nu(A)$ as a function of fragment mass A . The suggested shape of the neutron multiplicity curve in the lower part of the figure conforms surprisingly well with experiment.

The investigation both in experiment and theory of the energy spectra of neutrons from fission has a long history and is still going on. To good approximation it is assumed that in low energy fission the bulk of neutrons is evaporated from the fragments having reached their full speed. Fragments reach 90% of their final velocity in $\approx 5 \times 10^{-21} \text{s}$ while neutrons are evaporated in times $> 10^{-19} \text{s}$. For example, to evaporate a neutron with energy $E_n = 1 \text{ MeV}$ takes 10^{-18}s .

In experiment neutrons and their spectra are measured in the Lab system. From theory one expects that the transformation of an evaporation spectrum in the CM of fragments yields a Watt spectrum in the LAB. Somewhat surprisingly it turns out that in the LAB a Maxwell spectrum describes well the measured spectra of neutron energy E_n :

$$\Phi(E_n) \sim E_n^{1/2} \exp(-E_n/T)$$

with $\langle E_n \rangle = (3/2) T$ and $\sigma^2 = 2 \langle E_n \rangle^2 / 3$.

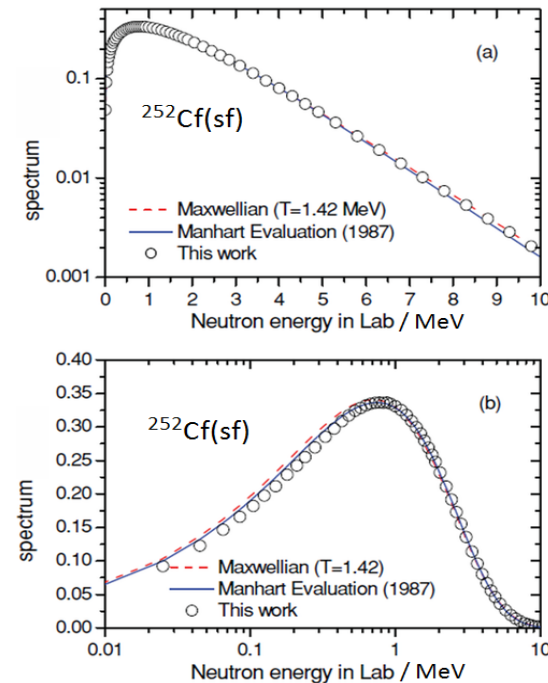
As demonstrated in the figures, the global spectrum for $^{252}\text{Cf}(sf)$ is well described by a Maxwell distribution. From a fit to the data the temperature is found to be $T = 1.42 \text{ MeV}$. This corresponds to an average energy $\langle E_n \rangle = 3/2 T = 2.13 \text{ MeV}$. The peak energy E_p is $E_p = T/2 = 0.71 \text{ MeV}$. The data are shown both on a linear (a) and a logarithmic energy scale (b) for the neutrons. On the linear scale the exponential decrease of neutron yield for energies E_n in excess of $E_n \approx 2 \text{ MeV}$ is evident. On the logarithmic scale more details of the low energy part of the spectrum come into view.

An important role in the discussion of neutron spectra plays the Manhart evaluation (1987) shown in the figure. It combines the work of several authors. The spectrum often serves as a reference.

In the figure besides the Manhart spectrum and its fit to a Maxwellian also theoretical results are displayed as open circles. The starting point for theory is the evaporation spectrum of neutrons as derived by Weisskopf in 1937. The spectrum for one neutron emitted in the CM of the moving fragment is given by

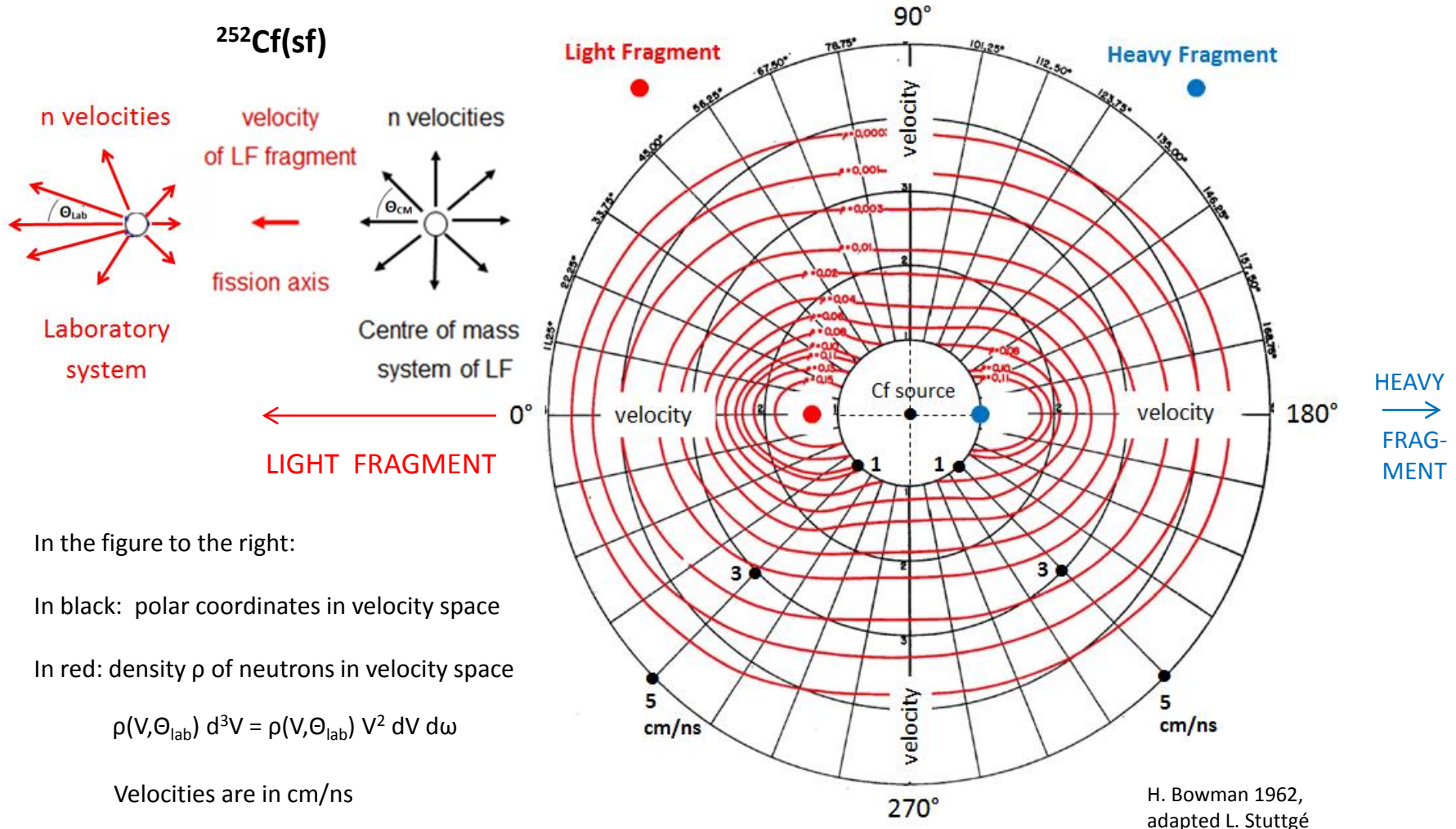
$$\varphi(\eta) \sim (\eta/T^2) \exp(-\eta/T)$$

with η the kinetic energy of neutrons in the CM system and T the temperature of the daughter nucleus. For the calculations the temperatures of the two fragments have to be known. Several recipes how the total excitation energy TXE is shared between the two fragments have been proposed. Theory describes very well experiment.



Angular and Velocity Distributions of Prompt Neutrons

In groundbreaking experiments H. Bowman et al demonstrated in 1962/63 that the bulk of prompt neutrons is evaporated isotropically from fragments having reached their full final speed. Evidence comes from the analysis of velocities and angular distributions of neutrons relative to the fission axis LIGHT \longleftrightarrow HEAVY as observed in the LAB system The velocity distribution is markedly non-isotropic: the neutron density as a function of velocity and angle relative to the fission axis is strongly shifted in direction of fragment flight. It is attributed to the isotropic distributions of neutron velocities in the CM systems of fragments with the shift in the LAB system coming about by the vector addition of neutron and fragment velocities. See figures.



In the figure to the right:

In black: polar coordinates in velocity space

In red: density ρ of neutrons in velocity space

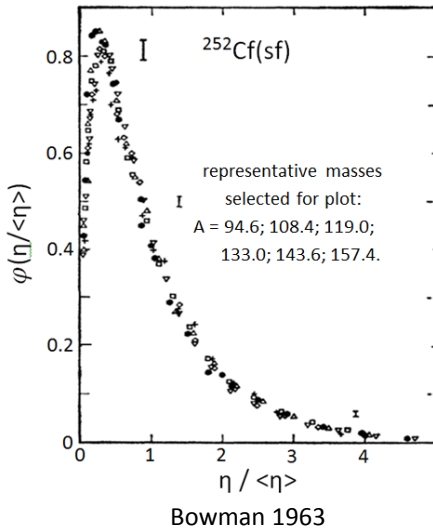
$$\rho(V, \theta_{\text{lab}}) d^3V = \rho(V, \theta_{\text{lab}}) V^2 dV d\omega$$

Velocities are in cm/ns

H. Bowman 1962,
adapted L. Stuttgé

While theory starts with the calculation of neutron data in the CM of fragments, in experiment data are measured in the LAB. For the transformation of neutron data obtained in the LAB to the CM system of fragments, and vice versa, the velocities of fragments have to be known. Velocities are determined by the fragment time-of-flight over a given distance. In the evaluation of experiments both, neutron energies E_n in the LAB and energies η in the CM of fragments are obtained as a function of fragment mass A and total kinetic energy TKE, event by event. Hence $E_n = E_n(A, TKE)$ in the LAB and $\eta = \eta(A, TKE)$ in the CM system are found.

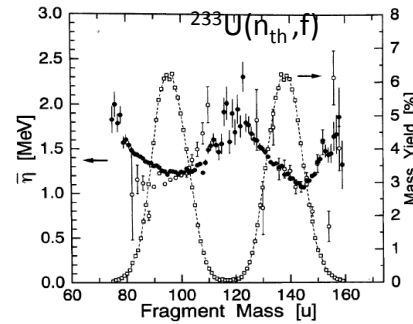
In the evaluation performed by Bowman et al. fission neutrons are evaporated from the two fragments having reached their full



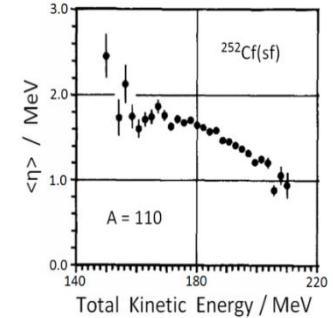
speed. The neutron spectra $\varphi(\langle\eta(A)\rangle)$ in the CM are obtained. An interesting result is that spectra $\varphi(\langle\eta(A)\rangle)$ averaged over TKE have the same shape for all masses A . This is visualized in the figure for $^{252}\text{Cf}(sf)$. All spectra $\varphi(\langle\eta(A)\rangle)$ are subsumed in one universal spectrum $\varphi(\eta)$ when normalized to unity and plotted versus the normalized variable $\eta / \langle\eta\rangle$.

Similar results were found for the reactions ^{233}U and $^{235}\text{U}(n_{th}, f)$ analyzed by Nishio in 1998. An example is on display for $^{233}\text{U}(n, f)$. Shown are average energies $\langle\eta(A)\rangle$ as a function of fragment mass A . For comparison also the mass yield $Y(A)$ is given. In most cases the CM energy lies between 1.3 and 1.4 MeV. For symmetric and super-asymmetric fission the CM energies reach maxima with $\langle\eta(A)\rangle$ coming close to 2.0 MeV. Remarkably, already back in 1966

H.W. Schmitt pointed for the reaction $^{235}\text{U}(n_{th}, f)$ to large excitation energies $TXE = Q^* - TKE^*$ close to $TXE = 40$ MeV for both, symmetric and superasymmetric fission.



Nishio 1998



Budtz-Jørgensen 1988

As to the energy dependence of $\eta(A, TKE)$, an example is provided for the mass $A = 110$ in fission of ^{252}Cf (figure to the right). The neutron energy decreases for increasing kinetic energy TKE of fragments and hence increases with excitation energy TXE. The result confirms expectation.

Though the transformation laws between neutron spectra in the LAB and the CM systems lead to rather complex expressions, there is a simple relation for the global average energies $\langle E_n \rangle$ and $\langle \eta \rangle$:

$$\langle E_n \rangle = \langle \eta \rangle + \langle E_f \rangle$$

with E_f the fragment kinetic energy per nucleon.

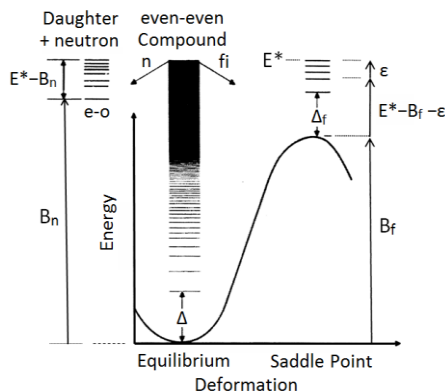
Remarkably the knowledge of neutron multiplicity ν and kinetic energy η in the CM system allows to find the average total excitation $\langle E_{ntot} \rangle$ drained by neutrons

$$\langle E_{ntot} \rangle = \langle \nu \rangle (\langle B_n \rangle + \langle \eta \rangle)$$

with $B_n \approx 5.5$ MeV the binding energy of neutrons.

$^{235}\text{U}(n_{th}, f)$: $\langle E_{ntot} \rangle \approx 17$ MeV. $^{252}\text{Cf}(sf)$: $\langle E_{ntot} \rangle \approx 26$ MeV

Irradiating heavy nuclei in the actinides with very low energy neutrons, e.g. thermal neutrons, the absorption of a neutron leads to the always present capture (n, γ) reaction and in case of fissile target nuclei in addition to the fission reaction (n,f). At higher incident energies in the MeV range, following neutron capture fission has to compete with neutron re-emission. This is schematically illustrated in the figure for an e-e compound nucleus. E^* is the excitation energy of the nucleus. In the fission sector to the right B_f , Δ_f , and ϵ are the fission barrier, the pairing energy gap in the level density of the fissioning nucleus and the kinetic energy in the fission degree of freedom, respectively. The intrinsic energy of excitation at the saddle point is ($E^* - B_f - \epsilon$). In the neutron sector to the left B_n is the neutron binding energy while ($E^* - B_n$) is the excitation energy of the e-o daughter nucleus having evaporated a neutron. The relative probabilities of decay are quantified by the decay widths Γ_f and Γ_n for fission and neutron emission, respectively. The relative probabilities of decay are approximately given by



Vandebosch-Huizenga 1973

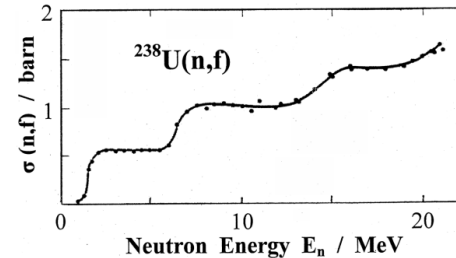
and neutron emission, respectively. The relative probabilities of decay are approximately given by

$$\Gamma_n / \Gamma_f \sim \exp\{-(B_n - B_f)\}.$$

For fissile nuclei like ^{235}U the difference is $(B_n - B_f) > 0$ (see figure) while for fertile nuclei like ^{238}U one has $(B_n - B_f) < 0$.

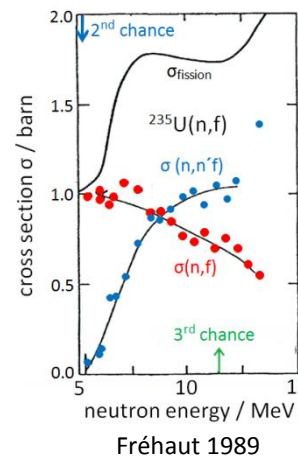
It should be recalled that besides the (n,f) and the (n, γ) reactions, where the incoming neutron is absorbed, neutrons may be scattered elastically or inelastically in (n,n) or (n,n') reactions.

A typical example for the fission cross section (n,f) at higher excitation energy is on display for the target ^{238}U .



The stepwise increase of the cross section $\sigma(n,f)$ with incident neutron energy is startling. The explanation is straightforward. For

the non-fissile nucleus ^{238}U the fission barrier of ^{239}U is $B_f \approx 6.1$ MeV and thus larger than the neutron binding $B_n \approx 4.8$ MeV gained by neutron capture. For the fission cross section to become sizable the missing 1.3 MeV has to be supplied by the kinetic energy of the incoming neutron. Further increasing the neutron energy the cross section stays constant for about 5 MeV until a second step at ≈ 6.5 MeV indicates that the threshold for a new process has been reached. In the new process a neutron may be emitted from the compound ^{239}U but still enough energy being left to overcome the fission barrier of the daughter



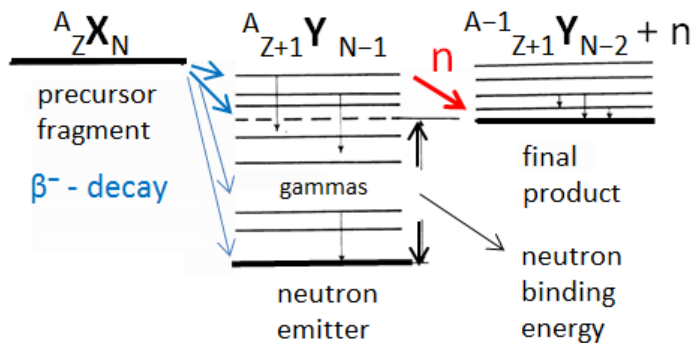
^{238}U . There are thus two processes contributing to fission: "first chance fission" (n,f) and "second chance fission" (n,n').

In the figure the onset of 2nd and also 3rd chance fission is marked by arrows for the fissile target nucleus ^{235}U . The contributions of 1st and 2nd chance fission are shown separately. Note the offset of the energy scale.

Most neutrons are evaporated in times smaller than a few 10^{-14} s. These are called prompt neutrons. A second fraction of neutrons is showing up at much later times starting at about 1 ms after fission. These late neutrons are therefore called “delayed neutrons”.

After prompt neutron emission the “primary” fragments have become “secondary” fragments. As a rule these latter fragments are still too n-rich and hence unstable. To reach the stability line of the nuclide chart they undergo β^- -decay. The β^- -decay is induced by the weak interaction and the corresponding reaction times are long. For secondary fragments showing up in fission the β^- -decay times range from ~ 1 ms to times much longer than the age of the universe. For many of the fragments β^- -decay leads in the daughter nucleus to excitation energies in excess of the neutron binding energy. In these cases – besides delayed gammas – delayed neutrons may be emitted.

In emission of delayed neutrons the nuclei involved are the n-precursor fragment ${}^A_Z X_N$, following β^- -decay the neutron emitter ${}^A_{Z+1} Y_{N-1}$ and following n-emission the final product ${}^{A-1}_{Z+1} Y_{N-2} + n$. The level schemes illustrate cases favorable for the emission of delayed neutrons.



The number N_β of β^- -decays per fission in (n_{th}, f) -reactions of actinides is $N_\beta = 6.0 \pm 0.5$. Among the fission products about 300 nuclei are precursors to emission of neutrons. Most delayed neutrons appear within 1 min after fission. They are of crucial importance for the safe operation of power reactors. To simplify the analysis they are lumped together into 6 groups according to their half-lives $T_{1/2}$. Delayed neutron data are given in the table. The characteristic parameters are the half-lives $T_{1/2}$, average neutron energies $\langle E_n \rangle$ and probabilities P_k in % for the six groups labeled k. They are shown in the table.

k	$T_{1/2}/s$	E_n/MeV	$P_k/\%$
1	53.0	0.41	3.5
2	21.6	0.47	18.1
3	5.3	0.44	17.3
4	2.3	0.56	38.7
5	0.83	0.52	15.6
6	0.25	0.54	6.6

D.E. Cullen 2004

Averaged over all groups the half-life for delayed neutrons from thermal fission of ${}^{235}U$ is

$$\langle T_{1/2} \rangle = 9.0 \pm 1.0 \text{ s}$$

Energy spectra of delayed neutrons are parameterized as Maxwellians

$$P(E_n) \sim E_n^{1/2} \exp(-E_n/T) \text{ with } \langle E_n \rangle = 3T/2$$

The average $\langle E_n \rangle$ of the energies on display in the table is

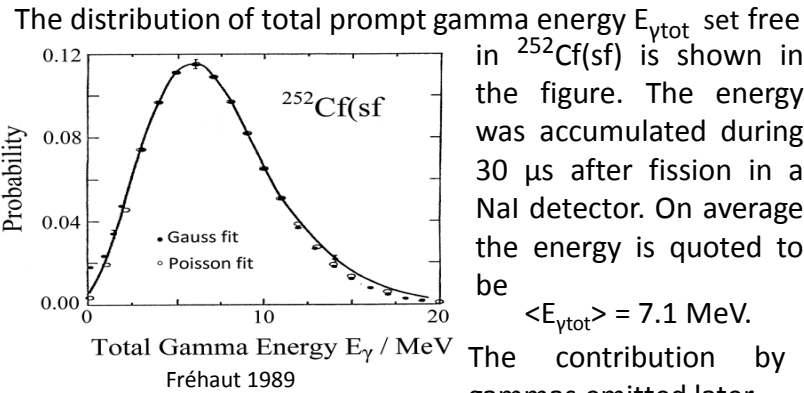
$$\langle E_n \rangle = 0.51 \text{ MeV}$$

For thermal neutron fission of ${}^{235}U$ and ${}^{239}Pu$ the ratio

$$\beta = v_{del}/v_{tot} \text{ with } v_{tot} = v_{prompt} + v_{delayed}$$

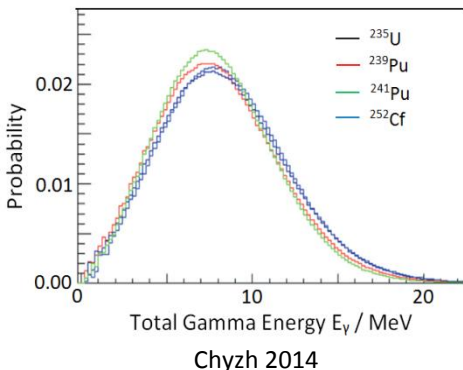
is $\beta = 0.65\%$ and $\beta = 0.24\%$, respectively.

Total γ -ray energy $E_{\gamma\text{tot}}$



than 30 μs is negligibly small.

In a comparative study of low energy n-induced fission of ^{235}U , ^{239}Pu and ^{241}Pu , and spontaneous fission of ^{252}Cf the total γ -ray energy E_{γ} was measured with the spectrometer DANCE from LANSCE in a time window of 40 ns after fission.



The contribution by gammas emitted later

As γ -detectors served 160 BaF_2 scintillators. As borne out in the figure, the distributions of E_{γ} for the four reactions analyzed are very similar. A remarkable result is obtained for the average total γ -energy $\langle E_{\gamma\text{tot}} \rangle$ which exceeds all former measurements by 20 %. For example, for $^{252}\text{Cf(sf)}$ the average $\langle E_{\gamma} \rangle$ is reported to be $\langle E_{\gamma\text{tot}} \rangle = 8.52 \text{ MeV}$. Taking the short time window of gamma observation into account this figure is rather a lower limit to the γ -energy release. Since prompt gammas contribute to the heating of reactor cores a precise knowledge of the energy release $\langle E_{\gamma\text{tot}} \rangle$ is of great practical importance.

Contributions to TXE

Discussing the total available excitation energy TXE in fission the relation

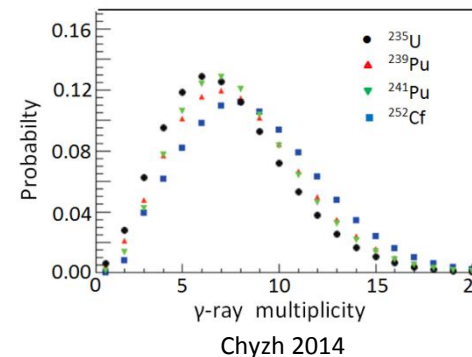
$\text{TXE} = v_{\text{tot}} \cdot [B_n + \eta] + E_{\gamma\text{tot}} = E_{\text{ntot}} + E_{\gamma\text{tot}}$ was introduced. Here v_{tot} , B_n , η and $E_{\gamma\text{tot}}$ are the total neutron multiplicity, the neutron binding energy in the fragments, the neutron kinetic energy in the CM system of fragments and the total gamma energy, respectively. For two reactions the contributions are detailed. Throughout

Reaction	v_{tot}	B_n	η	$E_{\gamma\text{tot}}$	$E_{\text{ntot}} + E_{\gamma\text{tot}}$
$^{235}\text{U}(n_{\text{th}}, f)$	2.43	5.5	1.4	8(1)	24.8(20)
$^{252}\text{Cf(sf)}$	3.76	5.5	1.4	8(1)	33.9(20)

average values are given with energies in MeV. Evidently, variations of TXE are reflected in the neutron multiplicity v_n .

Gamma multiplicity M_{γ}

Gamma multiplicities M_{γ} for thermal neutron induced and spontaneous fission are very similar. This is brought to evidence in the comparative study already addressed in connection with the total γ -energy output E_{γ} . In the four



reactions under study up to 20 γ -quanta per fission are observed. The largest differences between average multiplicities are between $^{235}\text{U}(n, f)$ with $\langle M_{\gamma} \rangle = 7.35$ and ^{252}Cf with $\langle M_{\gamma} \rangle = 8.75$. A rough estimate for the

average energy $\langle \epsilon \rangle$ of single gamma quanta is obtained from $\langle \epsilon \rangle \approx \langle E_{\gamma} \rangle / \langle M_{\gamma} \rangle$. The energies are $\langle \epsilon \rangle = 1.0(1) \text{ MeV}$.

$^{252}\text{Cf}(sf)$

Compared to many other topics in fission, gamma emission has not been much studied. Measurements are difficult because γ -energies range from a few tens of keV up to 10 MeV and the emission times vary from 10^{-14} s up to 1 ms. Most data have been taken for times within 10 ns after fission. The best studied reactions up to date still are $^{252}\text{Cf}(sf)$ and $^{235}\text{U}(n_{th},f)$.

Of prime interest are the energies ϵ_γ of individual photons and their multiplicity M_γ . In recent comprehensive studies the gamma emission from $^{252}\text{Cf}(sf)$ was studied and compared to data taken 40 years earlier. Gamma spectra were taken by different detector types:

Blue: NaI(Tl); 1973

Red: $\text{LaBr}_3:\text{Ce}$; 2013

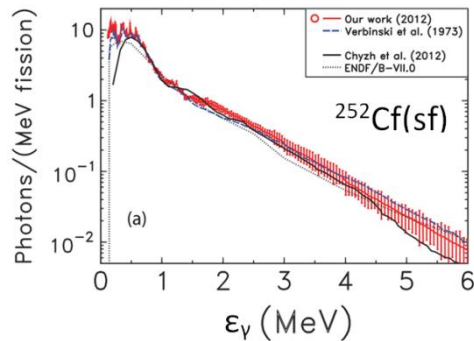
Curve: BaF_2 ; 2012

For the bulk of quanta:
 $0.3 < E_\gamma < 1.0$ MeV.
Time window: < 10 ns.

Blue: Verbinski 1973

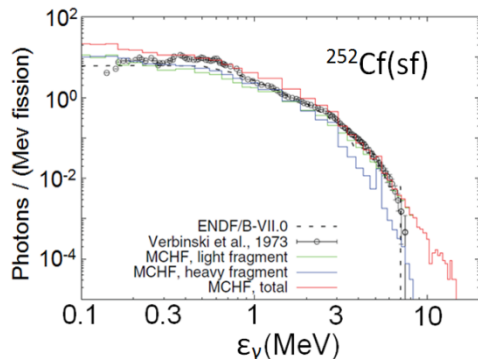
Curve: Chyzh 2012

Red: Billnert 2013,



The gamma-spectrum is well described by theory as brought to evidence in the figure for the reaction $^{252}\text{Cf}(sf)$. Plotted are experimental results

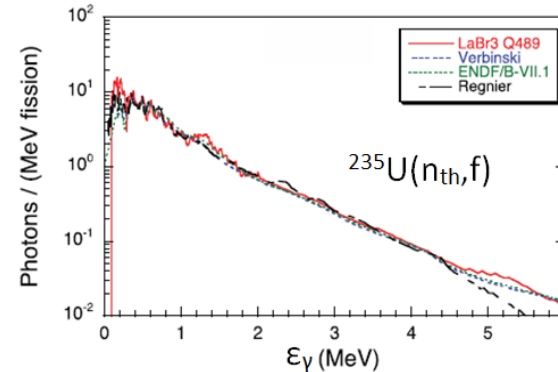
(circles Verbinski 1973), evaluated data (dotted ENDF/B-VII.0) and theoretical results (histograms for light and heavy fragment, and total from Monte-Carlo Hartree-Fock model).



Becker 2013 theory

$^{235}\text{U}(n_{th},f)$

The gamma spectrum observed in the standard reaction $^{235}\text{U}(n_{th},f)$ is not much different from the one in (sf) decay of ^{252}Cf . In going from gamma energies ϵ_γ near $\epsilon_\gamma = 1$ MeV

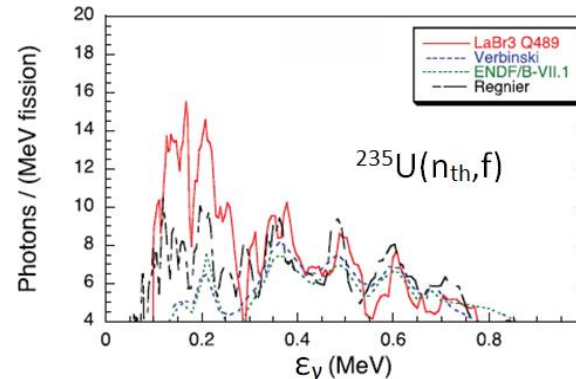


Detectors:
Blue: NaI(Tl)
(Verbinski 1973)
Red: $\text{LaBr}_3:\text{Ce}$
(Oberstedt 2013)
Dashed: theory
Regnier 2013

A. Oberstedt 2013

to $\epsilon_\gamma = 6$ MeV the emission probability decreases smoothly exponentially by 4 orders of magnitude. Only at low energies $\epsilon_\gamma < 1$ MeV a fine structure shows up.

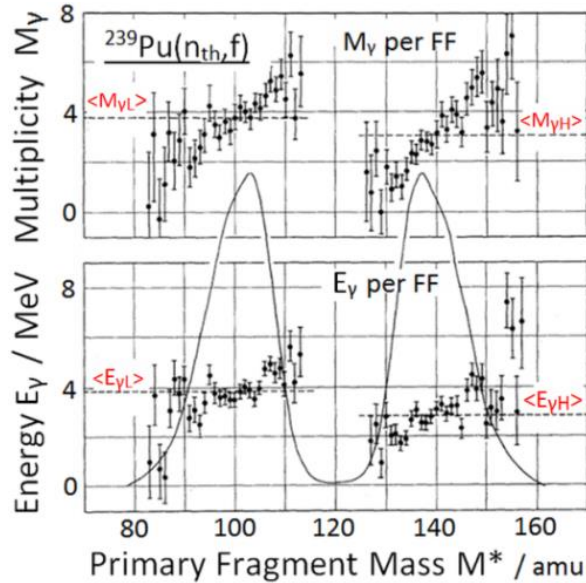
This structure becomes convincing in a zoom for gamma energies below 1 MeV. The structure was already observed in 1957 [Voitovetskii], established in 1973 [v. Verbinski] and corroborated with high resolution 40 years later. The structure is attributed to collective rotational levels of (e,e) fission fragments.



Detectors:
Blue: NaI(Tl)
(Verbinski 1973)
Red: $\text{LaBr}_3:\text{Ce}$
(Oberstedt 2013)
Dashed: theory
Regnier 2013

A. Oberstedt 2013

Gamma energy E_γ and multiplicity M_γ of photons as a function of fragment masses was investigated for several standard (n_{th},f) and (sf) reactions. A typical example is on display for $^{239}\text{Pu}(n_{th},f)$. For a time window of less than 5 ns

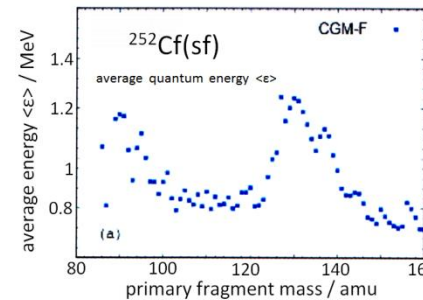
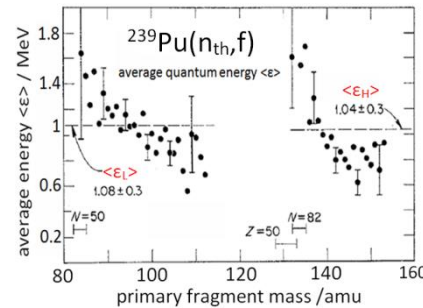


Pleasanton 1973

the multiplicity M_γ has the same sawtooth behaviour as the neutron multiplicity ν_n . Likewise the total average gamma energies $\langle E_\gamma \rangle$ per FF follow in shape a sawtooth vs. fragment mass. For the reaction $^{252}\text{Cf}(sf)$ see [Nardi 1973].

The saw-tooth shapes of multiplicity *versus* fragment mass are similar for both, neutrons and gammas. They have in fact as a common root the deformation of fragments at scission. Take e.g. the mass $A_{LF} = 110$ in $^{240}\text{Pu}^*$: for neutrons it is the large energy stored in the large deformation which is counting while for gammas large deformations lead to large angular momenta of fragments having to be exhausted by more than average numbers of photons.

In contrast to γ -multiplicity $M_\gamma(A)$ the plot of the quantum energy $\langle \epsilon(A) \rangle$ vs. fragment mass looks like an anti-saw-tooth. The wider level spacing for magic fragments obviously entails low γ -multiplicity but large quantum energies $\langle \epsilon(A) \rangle$.



Experiment $^{239}\text{Pu}(n_{th},f)$:

The average photon energy as a function of fragment mass $\langle \epsilon(A) \rangle$ exhibits an anti-sawtooth. The total γ -energy $\langle E_\gamma(A) \rangle = \langle M_\gamma(A) \rangle \cdot \langle \epsilon_\gamma(A) \rangle$ is therefore a rather flat function of fragment mass A.

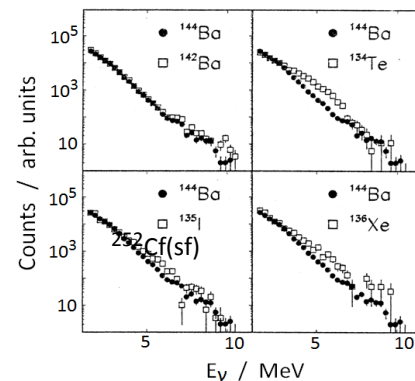
Pleasanton 1973

The actinide targets ^{233}U , ^{235}U and ^{239}Pu studied in thermal neutron fission and (sf) of ^{252}Cf exhibit similar features for $\langle \epsilon(A) \rangle$. As shown for $^{252}\text{Cf}(sf)$ theory describes well the structure of $\langle \epsilon(A) \rangle$ versus fragment mass A.

Talou 2013

Peculiarities for magic fragments

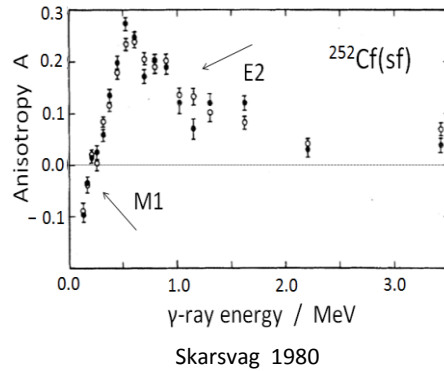
The γ -spectra for virtually all fragments are very similar. There is, however, an exception for magic fragments. For example in $^{252}\text{Cf}(sf)$ these nuclei exhibit an enhancement of γ -yield at energies ϵ_γ near 5 MeV. This is attributed to the wider spacing of levels in magic nuclei. At given excitation energy this will favor the emission of hard photons.



Biswas 1999

Anisotropy of Gamma Emission

Very early in the history of fission it was discovered that the emission of gammas is non-isotropic relative to the fission axis.



This was found for all low energy fission reactions studied. An example is shown in the figure for $^{252}\text{Cf}(sf)$. The anisotropy A is defined as $A = [W(0^\circ) - W(90^\circ)] / W(90^\circ)$ for the angle $\theta_{\gamma f}$ between the gamma and the fi-axis.

The anisotropy measured varies strongly with γ -energy. For low-energy gammas with $E_\gamma < 200$ keV the anisotropy A is $A < 0$ with more gammas emitted at $\theta = 90^\circ$ perpendicular to the fission axis than along the fission axis at $\theta = 0^\circ$. The anisotropy changes sign for the majority of gammas with energies $E_\gamma > 200$ keV. For positive $A > 0$ gammas are preferentially emitted along the fission axis.

A succinct interpretation of the anisotropy was given by V. Strutinski in 1960. It is pointed out that the sizable angular momenta carried by the fragments are oriented in a plane perpendicular to the fission axis. The probability for emission of gammas is a function of the angle $\theta_{\gamma I}$ between the gamma and fragment spin I . After averaging over all orientations of spin around the fission axis the angular distribution $W(\theta)$ becomes a function of the angle $\theta_{\gamma f}$ between the gamma and the fission axis in the CM system of the fragment. To each multipole L of the radiation field thereby belongs a characteristic angular emission pattern.

According to Strutinski the angular distribution $W(\theta_{\gamma I})$ of gammas relative to fragment spin I reads

$$W_{L=1}(\theta_{\gamma I}) \approx 1 + \frac{1}{4}(\hbar^2 J / \mathfrak{I} T)^2 \cos^2 \theta_{\gamma I} \text{ for } L = 1 \text{ (dipole) and}$$

$W_{L=2}(\theta_{\gamma I}) \approx 1 - \frac{3}{4}(\hbar^2 J / \mathfrak{I} T)^2 \cos^2 \theta_{\gamma I}$ for $L = 2$ (quadrupole) with \mathfrak{I} the moment of inertia and T the temperature. The already mentioned averaging over the orientations of I may be shown to yield

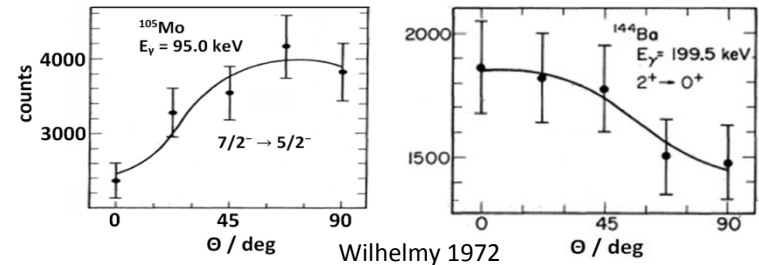
$$\langle \cos^2 \theta_{\gamma I} \rangle = \frac{1}{2} \sin^2 \theta.$$

The angular distributions $W_L(\theta_{\gamma f})$ relative to the fission axis are

$$W_{L=1}(\theta_{\gamma f}) \approx 1 + \frac{1}{8}(\hbar^2 J / \mathfrak{I} T)^2 \sin^2 \theta_{\gamma f} \text{ for } L = 1 \text{ (dipole) and}$$

$$W_{L=2}(\theta_{\gamma f}) \approx 1 - \frac{3}{8}(\hbar^2 J / \mathfrak{I} T)^2 \sin^2 \theta_{\gamma f} \text{ for } L = 2 \text{ (quadrupole).}$$

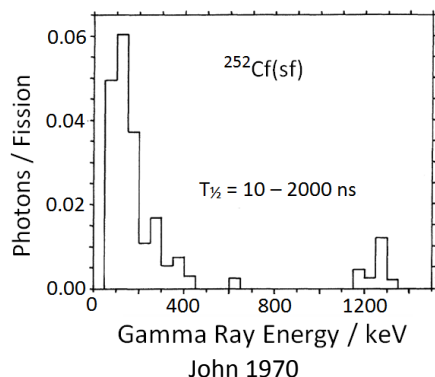
Note that the anisotropy A is negative for dipole and positive for quadrupole gammas. This could explicitly be verified by studying the anisotropy for single transitions between known levels in the $^{252}\text{Cf}(sf)$ reaction as shown in the figure. To the



left the M1 dipole gammas to the groundstate of ^{105}Mo are preferentially emitted perpendicular to the fission axis, while the E2 quadrupole gammas to the groundstate of ^{144}Ba favor emission along the fission axis. It has to be pointed out that the above angular distribution from theory pertain to the emission in the CM system of fragments while the experimental results are obtained in the LAB system. Yet the transformation from the CM to the LAB system will not change the characteristics of the angular distributions.

Gammas emitted in times > 50 ns after scission may be called “late” gammas. They should not be confounded with β -delayed gammas emitted following β -decay by daughter nuclei left in an excited state. Late gammas presently to be discussed stem from isomeric states of fragments having been excited in the course of fission.

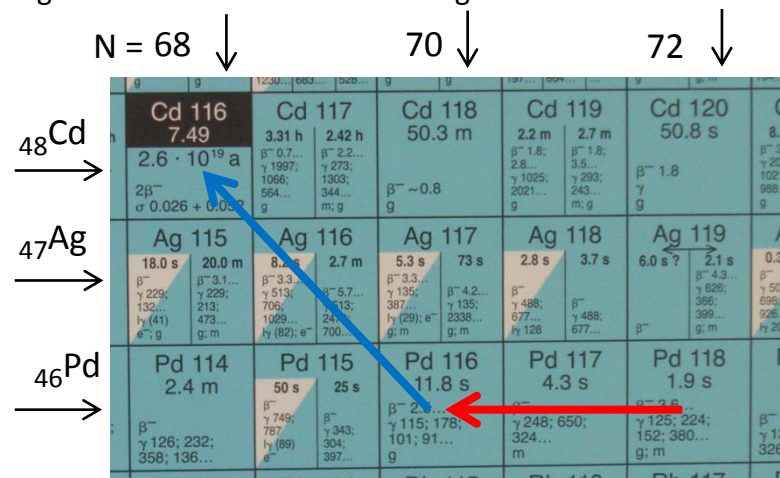
Searching for late gammas, in a study of spontaneous fission of ^{252}Cf the time window of γ -detection was extended from 3 ns to 2000 ns. The figure due to W. John (1970) shows γ -spectra in the time range 10 ns to 2000 ns. Remarkably, long-living isomers, albeit with small yields, show up for two different ranges of γ -energy: for low energies below 500 keV and for very high energies near 1250 keV. It is further found that these γ 's are preferentially emitted from fragments near mass 132. This mass number suggests the influence of magic shells like in ^{132}Sn . Microsecond isomers in the magic regions ^{78}Ni and ^{132}Sn have been extensively studied in recent years [Pinston 2004].



From the γ -anisotropy measurements discussed in the foregoing it is concluded that these high energy gammas have the multipolarity E2. They may possibly be interpreted as collective vibrations of stiff magic nuclei. However, they are by orders of magnitude

slower than anticipated. Most probably this tells that the quanta in question are fed by γ -cascades with a long-living spin isomer on top of the cascade.

discussed for symmetric fission of $^{235}\text{U}(n_{\text{th}},f)$ Following prompt neutron and prompt gamma emission the TXE is exhausted and the primary products have reached their ground states. However, as a rule, these states are not β^- stable. The reason is simple: for heavy nuclei like fissioning actinides the N/Z ratio is larger than for the medium-weight fission fragments and the available TXE is not sufficient to evaporate enough neutrons. Take symmetric fission of $^{235}\text{U}(n_{\text{th}},f)$ as an example. The two primary fragments are $^{118}\text{Pd}_{72}$. The energy at disposal is about TXE = 40 MeV. Per fragment this allows the evaporation of 2 neutrons per fragment. This is visualized in the figure. The two final



fragments are $^{116}\text{Pd}_{70}$. They have a half-life of 11.8 s for a first β^- decay to $^{116}\text{Ag}_{69}$, decaying further with half-lives up to 2.7 m to the stable Cd isotope $^{116}\text{Cd}_{68}$.

The β^- -decay of fission products is to a large extent responsible for the unavoidable radioactivity of nuclear waste from nuclear power stations.

Summary

- **Neutron-induced Fission** was studied almost exclusively in the actinides as targets
- **Essence of Nuclear Fission:** deformation of a nucleus up to a saddle point, the so-called fission barrier B_f .
Beyond barrier fission proceeds to scission point without coming back to ground state deformation.
In the actinides $B_f \approx 6$ MeV.
Basic theory : **Liquid Drop Model**.
- **Fragment Mass Distributions:** at low E_x asymmetric fission is dominant from Ac to light isotopes of Fm – No.
Asymmetric and superasymmetric fission. In heavy isotopes of Fm – Lr symmetric bimodal fission.
Theory: **LDM + Shell Model** stabilizing magic fragments , new magic numbers for deformed nuclei.
- **Fragment Kinetic Energies:** distinct modes in the $Y(A,E)$ distributions are linked to distinct paths in the PES.
Theory: **PES** with account of macroscopic and microscopic features
- **Fragment Charge Distributions:** at low E_x even-odd staggering with $Y(e-Z) > Y(o-Z)$ in particular for (e-Z) CN
Theory: **Pairing in Superfluidity**. In superasymmetric fission: fragment shells stabilize even-Z.
- **Neutron and Gamma Emission:** neutrons and gammas exhaust the excitation energies TXE of fragments.
First neutrons are emitted in times $< .. 10^{-14}$ s. Salient feature: sawtooth of n-multiplicity from FF(A).
Theory: **Deformability of Fragments**
Gammas are mostly emitted after neutrons in times from 10^{-14} s up to ~ 1 ms.
Spectroscopy of n-rich nuclei, shape and spin isomers, measurement of FF angular momentum.
Theory: **Level structure of n-rich nuclei**
- **β -decay of Fission Fragments:** fragments become fission **Products**. Lifetimes from ~ 1 ms to 10^{+14} s.
Beta- and subsequent gamma-decay of products is the source of radioactivity of nuclear waste.

Key references

Mass Distributions

- S. Bjornholm and J.E. Lynn :Rev. Mod. Phys. 52,725 (1980)
 L. Dematté, C. Wagemans, R. Barthélémy et al.: Nucl. Phys. A 617, 331 (1997)
 H. Goutte, J.F. Berger, P. Casoli et al.: Phys. Rev. C 71, 024316 (2005)
 F.-J. Hamsch, S. Oberstedt, A. Tudora et al.: Nucl. Phys. 726, 248 (2003)
 M. Huhta, P. Dendooven, A. Honkanen et al.: Phys. Lett. B 405, 230 (1997)
 ILL collaboration in "The Neutron" by H. Börner and F. Gönnerwein, WS 2012
 R.C. Jensen and A.W. Fairhall: Phys. Rev. 109, 942 (1958)
 H.-H. Knitter, F.J. Hamsch, F. J. Budtz-Jorgensen et al.: Z. Naturf. 42a,786 (1987)
- P. Möller, A.J. Sierk, T. Ichikawa et al.: Phys. Rev. C 79, 064304 (2009)
 S. Nagy, K.F. Flynn, J.E. Gindler et al.: Phys. Rev C17, 163 (1978)
 E. Pfeiffer: Z. Physik 240, 403 (1970)
 D. Rochman, I. Tsekhanovich, F. Gönnerwein et al.: Nucl. Phys. 735, 3 (2004)
 I. Tsekhanovich, H.-O. Denschlag, M. Davi et al.: Nucl. Phys. A 688, 633 (2001)
 J.P. Unk, J.E. Gindler, J.E. Glendenin et al.: Proc. IAEA Vienna, Vol. II, 20 (1974)

Energy Distributions

- P. Geltenbort: PHD thesis Univ. of Tübingen, 1985, unpublished
 F. Gönnerwein in "The Nuclear Fission Process", C. Wagemans ed., CRC Press 1991
 J.C.D. Milton and J.S. Fraser: Phys. Rev. 111, 877 (1958)
 A. Möller, F. Gönnerwein, J. Kaufmann et al.: Proc. "Sem. on Fission",
 C. Wagemans ed., Pont d'Oye 1995, EUR 16295 EN, p 76
 W. Mollenkopf, J. Kaufmann, F. Gönnerwein et al.: J. Phys. G 18, L203 (1992)
 A. Ruben and H. Märten: Proc. "Dyn. Aspects of Nuclear Fission", Dubna 1992
 H.W. Schmitt, J.H. Neiler and F.J. Walter: Phys. Rev. 111, 1146 (1966)

Charge Distributions

- J.P. Bocquet and R. Brissot: Nucl. Phys. 502, 213c (1989)
 F. Gönnerwein: Nucl. Instr. Meth A 316, 405 (1992)
 U. Quade, K. Rudolph, S. Skorka et al.: Nucl. Phys. 487, 1 (1988)
 P. Schillebeeckz, C. Wagemans, P. Geltenbort et al.: Nucl. Phys. A 580,15(1994)
 J.L. Sida, P. Armbruster, M. Bernas et al.: Nucl. Phys. 502, 233c (1989)

Neutrons and Gammas

- B. Becker, P. Talou, T. Kawano et al.: Phys. Rev. C 87, 014617 (2013)
 R. Billnert, F.-J. Hamsch, A. Oberstedt et al.: Phys. Rev. C 87, 024601 (2013)
 D.C. Biswas, B.K. Nayak, M. Cinausero et al.: Eur. Phys. J. A 4, 343 (1999)
 H.R. Bowman, S.G. Thompson, J.C.D. Milton et al.: Phys. Rev. 126, 2120 (1962)
 H.R. Bowman, J.C.D. Milton, S.G. Thompson et al.: Phys. Rev. 129, 2133 (1963)
 C. Budtz-Jørgensen and H.H. Knitter: Nucl. Phys. A 490, 307 (1988)
 A. Chyzh, C.Y. Wu, E. Kwan et al.: Phys. Rev. C 87, 034620 (2013)
 A. Chyzh, C.Y. Wu, E. Kwan et al.: Phys. Rev. C 90, 014602 (2014)
 J. Fréhaut: Proc. "Nuclear Data for Science and Technology", Mito 1988,
 IAEA 1989, p 81
 D. Hilscher and H. Rossner: Ann. Phys. (Paris) 17, 471 (1992)
 W. John, F.W. Guy and J.J. Wesolowski: Phys. Rev C 2, 1451 (1970)
 O. Litaize and O. Serot: Phys. Rev. 82, 054616 (2010)
 K. Nishio, Y. Nakagome et al.: Nucl. Phys. A 632, 540 (1998)
 A. Oberstedt, T. Belgia, R. Billnert et al.: Phys. Rev. C 87, 051602 (2013)
 F. Pleasonton: Nucl. Phys. A 213, 413 (1973)
 D. Regnier, O. Litaize and O. Serot: Phys. Proc. 31, 59 (2012)
 K. Skarsvag: Phys. Rev. C 22, 638 (1980)
 P. Talou, T. Kanon and I. Stet: Phys. Proc. 47, 39 (2013)
 J. Terrell: Phys. Rev. 108, 784 (1957)
 R. Vandenbosch and J.R. Huizenga: "Nuclear Fission", Academic Press 1973
 V.V. Verbinski, H. Weber and R.E. Sund: Phys. Rev. C 7, 1173 (1973)
 A.S. Vorobyev, V.N., Dushin, F.-J. Hamsch et al.: Proc. "Interactions
 of Neutrons with Nuclei", Dubna 2001, p 276
 A.S. Vorobyev, O.A. Shcherbakov, Yu. S. Pleva et al.: Proc. "Interactions
 of Neutrons with Nuclei", Dubna 2009, p 60
 J.B. Wilhelmy, E. Cheifetz, J.R.C. Jared et al.: Phys. Rev. C 5, 201 (1972)